PHYSICAL REVIEW D **89,** 093004 (2014)

Neutrino mass textures and partial μ–τ symmetry

E. I. Lashin,[1,2,3,*] N. Chamoun,[4,5,†] C. Hamzaoui,[6,‡] and S. Nasri[7,8,§]

[1]*Ain Shams University, Faculty of Science, Cairo 11566, Egypt*
[2]*Centre for Theoretical Physics, Zewail City of Science and Technology, Sheikh Zayed, 6 October City, 12588 Giza, Egypt*
[3]*The Abdus Salam ICTP, P.O. Box 586, 34100 Trieste, Italy*
[4]*Physics Department, HIAST, P.O. Box 31983, Damascus, Syria*
[5]*Physikalisches Institut der Universität Bonn, Nußalle 12, D-53115 Bonn, Germany*
[6]*Département des Sciences de la Terre et de L'Atmosphère, Groupe de Physique Théorique des Particules, Université du Québec à Montréal, Case Postale 8888, Succ. Centre-Ville, Montréal, Québec H3 3P8, Canada*
[7]*Department of Physics, UAE University, P.O. Box 17551, Al-Ain, United Arab Emirates*
[8]*Laboratoire de Physique Théorique, ES-SENIA University, DZ-31000 Oran, Algeria*

(Received 26 November 2013; published 7 May 2014)

We discuss the viability of the μ–τ interchange symmetry imposed on the neutrino mass matrix in the flavor space. Whereas the exact symmetry is shown to lead to textures of a completely degenerate spectrum, which is incompatible with the neutrino oscillation data, introducing small perturbations into the preceding textures, inserted in a minimal way, leads, however, to four deformed textures representing an approximate μ–τ symmetry. We motivate the form of these "minimal" textures, which disentangle the effects of the perturbations, and present some concrete realizations assuming exact μ–τ at the Lagrangian level but at the expense of adding new symmetries and matter fields. We find that all of these deformed textures are capable of accommodating the experimental data, and in all types of neutrino mass hierarchies, particularly the nonvanishing value for the smallest mixing angle.

DOI: 10.1103/PhysRevD.89.093004 PACS numbers: 14.60.Pq, 11.30.Hv, 14.60.St

I. INTRODUCTION

The elusive neutrino particles have proved, so far, to be the only feasible window for the physics beyond the standard model (SM) of particle physics. The observed solar and atmospheric neutrino oscillations in the Super-Kamiokande [1] experiment constitute compelling evidence for the massive nature of neutrinos, which is a clear departure from the SM particle physics. In the flavor basis where the charged lepton mass matrix is diagonal, the mixing can be solely attributed to the effective neutrino mass matrix M_ν. In such a case the neutrino mass matrix M_ν can be parametrized by nine free parameters: three masses (m_1, m_2, and m_3), three mixing angles (θ_x, θ_y, and θ_z), and three phases (two Majorana-type ρ, σ and one Dirac-type δ). The culmination of experimental data [2–5] amounts to constraining the masses and the mixing angles, while for the phases there is so far no feasible experimental set for their determination. The recent results from the T2K [6], MINOS [7], and Double Chooz [8] experiments reveal a nonzero value of θ_z. The more recent Daya Bay [9] and RENO [10] experiments confirm a sizable value with relatively high precision. The discovery of the relatively large mixing angle θ_z has a tremendous impact on searching for a sizable CP-violation effect in neutrino oscillations that enables measuring the Dirac phase δ. The impact could also extend to our understanding of matter-antimatter asymmetry that shaped our Universe.

In order to cope with a relatively large mixing angle θ_z, one might be compelled to introduce new ideas in model building that may enrich our theoretical understanding of the neutrino flavor problem or the flavor problem in general in case we are fortunate enough. One of the common ideas, often discussed in the literature [11], is using flavor symmetries, and one of the most attractive ideas in this regard is the μ–τ symmetry [12,13]. This symmetry is enjoyed by many popular mixing patterns such as tribimaximal mixing (TBM) [14], bimaximal mixing (BM) [15], hexagonal mixing (HM) [16], and scenarios of A_5 mixing [17], and it was largely studied in the literature [18]. Actually, many sorts of these symmetries happen to be "accidental"—just a numerical coincidence of parameters without underlying symmetry, but rather a symmetry resulting from a mutual influence of different and independent factors. The authors of [19] showed that the TBM symmetry falls under this category in that large deviations from its predictions are allowed experimentally. Nonetheless, one can adopt a more "fundamental" approach and construct models incorporating the symmetry in question at the Lagrangian level. In this context, recent, particularly simple, choices for discrete and continuous

*slashin@zewailcity.edu.eg
elashin@ictp.it
†nchamoun@th.physik.uni-bonn.de
‡hamzaoui.cherif@uqam.ca
§snasri@uaeu.ac.ae

 © 2014 American Physical Society

flavor symmetry addressing the nonvanishing θ_z question were respectively worked out in [20] and [21].

For the μ–τ symmetry, it is well known that the exact form often requires the vanishing θ_z and, thus, the recent results on the nonvanishing θ_z force us to abandon the idea of exact μ–τ symmetry and to invoke a small perturbation violating it. The idea of introducing perturbations over a μ–τ symmetric mass matrix was recently introduced in [22–24], where the authors analyzed the effect of perturbations and the correlation of their sizes with those corresponding to the deviation of θ_z and $\theta_y - \frac{\pi}{4}$ from zero. In [22], the perturbations are introduced into the μ-τ symmetric neutrino mass matrix at all entries, while in [23] the perturbations are introduced only at the mass matrix entries, which are related through μ–τ symmetry. The perturbations in [24] were imposed on four and three zero neutrino Yukawa textures. In fact, approximate interchange symmetry between second and third generation fields goes back to [25] where μ–τ symmetry was extended to all fermions with a concrete realization in a two-doublets Higgs model.

In this present work, we follow a similar procedure as in [23], and insert the perturbations only at mass matrix entries related by μ–τ symmetry. In our approach, however, the deformed relations are thought of as defining textures, and this way of thinking provides deep insight about the μ–τ symmetry itself and its breaking. The two relations defining the approximately μ–τ symmetric texture contain two parameters, generally complex, controlling the strength of the symmetry breaking. For the sake of simplicity and clarity, we disentangle each parameter to be kept alone in the relations defining the texture. The "minimal" textures obtained in this way (minimal in the sense of containing just one symmetry breaking parameter) may be considered as a "basis" for all perturbations. Moreover, the numerical study of [23] with a normal hierarchy spectrum required one of the two symmetry breaking parameters to be small with respect to the other, and this motivated us to consider the extreme case where one of the two symmetry breaking parameters is absent.

As we shall see, the exact μ–τ symmetry can be realized in two different ways as equating to zero two linear combinations of the mass matrix entries. Thus, upon deforming these two defining linear combinations, in each of the possible two ways of realizing μ–τ symmetry, by two parameters (each parameter affecting one linear combination) and separating the two parameters' effects, we end up with four possible textures. The two equations defining each texture provide us with four real equations, which are used to reduce the independent parameters of the neutrino mass matrix in this specific texture from nine to five. We choose the five input parameters to be the mixing angles $(\theta_x, \theta_y, \theta_z)$, the Dirac phase δ, and the solar mass square difference δm^2, and we vary them within their experimentally acceptable regions. Moreover, we vary the complex parameter defining the deformation. Therefore, in this way we can reconstruct the neutrino mass matrix out of seven-dimensional parameter space, and compute the unknown mass spectrum (m_1, m_2, m_3) and the two Majorana phases ρ and σ. We perform a consistency check with the other experimental results and find that all possible four textures could accommodate the data. However, no singular models, where one of the masses equals zero, could be viable.

In contrast to the analysis of [23], which stated that normal type hierarchy is not compatible with small perturbations ($\epsilon < 20\%$), we found all the patterns viable in all types of mass hierarchies (normal, inverted, and quasidegenerate) for even smaller perturbations ($\chi = 2\epsilon < 20\%$). The different conclusions are due to two factors. First, in [23] the phase angles are varied whereas the mixing angles and the other observables are fixed to their central values, which correspond to narrow slices in the parameter space we adopted in our work. Second, the definition of normal hierarchy in our work ($m_1/m_3 < m_2/m_3 < 0.7$) is less restricted than the definition adopted in [23] ($m_1 \ll m_2 \ll m_3$). Thus, we believe our analysis is more thorough and our conclusions are more solid.

As to the origin of the perturbations, there are a few strategies to follow. First, one can add terms explicitly violating the μ–τ symmetry in the Lagrangian, as was done in [26]. Second, one may assume exact symmetry, leading to $\theta_z = 0$, at the high scale. Then renormalization group (RG) running of the neutrino mass matrix elements creates a term that breaks the μ–τ symmetry at the electroweak scale. However, many studies showed that the RG effects are negligible. In [27], this process of symmetry breaking via RG running within a multiple Higgs doublets model was only valid, for a sizable θ_z, in a quasidegenrate spectrum. In [28], the same conclusion, about the inability of radiative breaking to generate a relatively large θ_z, was reached in minimal supersymmetric standard model (MSSM) schemes. Thus, we shall not consider RG effects, but impose approximate μ–τ symmetry at the high scale (the seesaw scale, say) which would remain valid at the measurable electroweak scale. Third, as was done in [29], the μ–τ symmetry is replaced by another symmetry including the former as a subgroup. In this spirit and in line with [23,25], we address in detail the question of the perturbations' root and present some concrete examples at the Lagrangian level for the minimal texture form which has only one breaking parameter by means of adding extra Higgs fields and symmetries, in both types I and II of seesaw mechanisms. In type II seesaw, we achieve the desired perturbed form by adding a new Z_2 symmetry to the one characterizing the μ-τ symmetry (which we denote henceforth by S) and three Higgs triplets responsible for giving masses to the left-handed (LH) neutrinos and by substituting three Higgs doublets for the SM Higgs field for the charged lepton masses. On the other hand, we achieve the desired form in type I seesaw by considering a flavor

symmetry of the form $S \times Z_8$ and by having three SM-like Higgs doublets for the charged leptons masses, four other Higgs doublets for the Dirac neutrino mass matrix, and additional two Higgs singlets for the Majorana right-handed (RH) neutrino mass matrix.

The plan of the paper is as follows: in Sec. II, we review the standard notation for the neutrino mass matrix and its relation to the experimental constraints. In Sec. III, we present the μ–τ symmetry and its implications. The realization of μ–τ symmetry as textures and its consequences for nonsingluar and singular cases are respectively worked out in Sec. IV and V. In Sec. VI, we present the minimal possible ways for breaking the μ–τ symmetry, leading to four cases being interpreted as four possible textures, and we classify all the hierarchy patterns regarding the mass spectra. The detailed relevant formulas and the results of the phenomenological analysis of each texture are presented in Section VII (for nonsingular cases) and Sec. VIII (for singular ones). In Sec. IX, we present a possible Lagrangian for the approximate μ–τ leading to the minimal textures we adopted. The last section, X, is devoted to discussions and conclusions.

II. STANDARD NOTATION

In the flavor basis, where the charged lepton mass matrix is diagonal, we diagonalize the symmetric neutrino mass matrix M_ν by a unitary transformation,

$$V^\dagger M_\nu V^* = \begin{pmatrix} m_1 & 0 & 0 \\ 0 & m_2 & 0 \\ 0 & 0 & m_3 \end{pmatrix}, \tag{1}$$

with m_i (for $i = 1, 2, 3$) being real and positive. We introduce the mixing angles $(\theta_x, \theta_y, \theta_z)$ and the phases (δ, ρ, σ) such that [30]

$$V = UP$$

$$P = \mathrm{diag}(e^{i\rho}, e^{i\sigma}, 1)$$

$$U = \begin{pmatrix} c_x c_z & s_x c_z & s_z \\ -c_x s_y s_z - s_x c_y e^{-i\delta} & -s_x s_y s_z + c_x c_y e^{-i\delta} & s_y c_z \\ -c_x c_y s_z + s_x s_y e^{-i\delta} & -s_x c_y s_z - c_x s_y e^{-i\delta} & c_y c_z \end{pmatrix} \tag{2}$$

(with $s_x \equiv \sin\theta_x \ldots$) to have

$$M_\nu = U \begin{pmatrix} \lambda_1 & 0 & 0 \\ 0 & \lambda_2 & 0 \\ 0 & 0 & \lambda_3 \end{pmatrix} U^T, \tag{3}$$

with

$$\lambda_1 = m_1 e^{2i\rho}, \qquad \lambda_2 = m_2 e^{2i\sigma}, \qquad \lambda_3 = m_3. \tag{4}$$

In this parametrization, the mass matrix elements are given by

$$\begin{aligned}
M_{\nu 11} &= m_1 c_x^2 c_z^2 e^{2i\rho} + m_2 s_x^2 c_z^2 e^{2i\sigma} + m_3 s_z^2, \\
M_{\nu 12} &= m_1(-c_z s_z c_x^2 s_y e^{2i\rho} - c_z c_x s_x c_y e^{i(2\rho-\delta)}) \\
&\quad + m_2(-c_z s_z s_x^2 s_y e^{2i\sigma} + c_z c_x s_x c_y e^{i(2\sigma-\delta)}) \\
&\quad + m_3 c_z s_z s_y, \\
M_{\nu 13} &= m_1(-c_z s_z c_x^2 c_y e^{2i\rho} + c_z c_x s_x s_y e^{i(2\rho-\delta)}) \\
&\quad + m_2(-c_z s_z s_x^2 c_y e^{2i\sigma} - c_z c_x s_x s_y e^{i(2\sigma-\delta)}) \\
&\quad + m_3 c_z s_z c_y, \\
M_{\nu 22} &= m_1(c_x s_z s_y e^{i\rho} + c_y s_x e^{i(\rho-\delta)})^2 \\
&\quad + m_2(s_x s_z s_y e^{i\sigma} - c_y c_x e^{i(\sigma-\delta)})^2 + m_3 c_z^2 s_y^2, \\
M_{\nu 33} &= m_1(c_x s_z c_y e^{i\rho} - c_y s_x e^{i(\rho-\delta)})^2 \\
&\quad + m_2(s_x s_z c_y e^{i\sigma} + s_y c_x e^{i(\sigma-\delta)})^2 + m_3 c_z^2 c_y^2, \\
M_{\nu 23} &= m_1(c_x^2 c_y s_y s_z^2 e^{2i\rho} + s_z c_x s_x(c_y^2 - s_y^2) e^{i(2\rho-\delta)} \\
&\quad - c_y s_y s_x^2 e^{2i(\rho-\delta)}) + m_2(s_x^2 c_y s_y s_z^2 e^{2i\sigma} \\
&\quad + s_z c_x s_x(s_y^2 - c_y^2) e^{i(2\sigma-\delta)} - c_y s_y c_x^2 e^{2i(\sigma-\delta)}) \\
&\quad + m_3 s_y c_y c_z^2.
\end{aligned} \tag{5}$$

Note that under the transformation given by

$$T_1 : \theta_y \to \frac{\pi}{2} - \theta_y \qquad \text{and} \qquad \delta \to \delta \pm \pi \tag{6}$$

the mass matrix elements are transformed amongst themselves by swapping the indices 2 and 3 and keeping the index 1 intact:

$$\begin{aligned}
&M_{\nu 11} \leftrightarrow M_{\nu 11}, \qquad M_{\nu 12} \leftrightarrow M_{\nu 13} \\
&M_{\nu 22} \leftrightarrow M_{\nu 33}, \qquad M_{\nu 23} \leftrightarrow M_{\nu 23}.
\end{aligned} \tag{7}$$

On the other hand, the mass matrix is transformed into its complex conjugate, i.e,

$$M_{\nu ij}(T_2(\delta, \rho, \sigma)) = M^*_{\nu ij}((\delta, \rho, \sigma)), \tag{8}$$

under the mapping given by

$$T_2 : \rho \to \pi - \rho, \qquad \sigma \to \pi - \sigma, \qquad \delta \to 2\pi - \delta. \tag{9}$$

The above two symmetries, $T_{1,2}$, are quite useful in classifying the models and in connecting the phenomenological analysis of patterns related by them.

It is straightforward to relate our parametrization convention, Eq. (2), to the more familiar one used in the recent data analysis of [31]. In fact, the mixing angles in the two parametrizations are equal,

TABLE I. The global-fit results of three neutrino mixing angles $(\theta_x, \theta_y, \theta_z)$ and two neutrino mass-squared differences δm^2 and Δm^2, as defined in Eq. (11). The results $[\cdots]$ and $(\cdots)$ are respectively extracted from [31] and [34]. In [31], it is assumed that $\cos\delta = \pm 1$ and that new reactor fluxes have been used, while in [34] δ is not restricted and the old reactor flux is used.

Parameter	Best fit	1σ range	2σ range	3σ range
$\delta m^2(10^{-5}\ \mathrm{eV}^2)$	7.58	[7.32,7.80]	[7.16,7.99]	[6.99,8.18]
$\lvert\Delta m^2\rvert(10^{-3}\ \mathrm{eV}^2)$	2.35	[2.26,2.47]	[2.17,2.57]	[2.06,2.67]
θ_x	33.58°	[32.96°,35.00°]	[31.95°,36.09°]	[30.98°,37.11°]
θ_y	40.40°	[38.65°,45.00°]	[36.87°,50.77°]	[35.67°,53.13°]
θ_z	8.33°	[7.71°,10.30°]	[6.29°,11.68°]	[4.05°,12.92°]
	8.99°	(8.45°,9.39°)	(7.99°,9.82°)	(7.47°,10.80°)
R_ν	0.0323	[0.0296,0.0345]	[0.0279,0.0368]	[0.0262,0.0397]

$$\theta_x \equiv \theta_{12}, \qquad \theta_y \equiv \theta_{23}, \qquad \theta_z \equiv \theta_{13}, \tag{10}$$

whereas there is a simple linear relation, discussed in [20,32], between the phases defined in our parametrization and those corresponding to the standard one.

The solar and atmospheric neutrino mass-squared differences are characterized by two independent neutrino mass-squared differences[31]:

$$\delta m^2 \equiv m_2^2 - m_1^2, \qquad |\Delta m^2| \equiv \left| m_3^2 - \frac{1}{2}(m_1^2 + m_2^2) \right|, \tag{11}$$

whereas the parameter

$$R_\nu \equiv \frac{\delta m^2}{|\Delta m^2|} \tag{12}$$

characterizes the hierarchy of these two quantities.

The neutrino mass scales are constrained in the reactor nuclear experiments on beta-decay kinematics and neutrinoless double-beta decay by two parameters that are the effective electron-neutrino mass,

$$\langle m \rangle_e = \sqrt{\sum_{i=1}^{3} (|V_{ei}|^2 m_i^2)}, \tag{13}$$

and the effective Majorana mass term $\langle m \rangle_{ee}$,

$$\langle m \rangle_{ee} = |m_1 V_{e1}^2 + m_2 V_{e2}^2 + m_3 V_{e3}^2| = |M_{\nu 11}|. \tag{14}$$

Another parameter with an upper bound coming from cosmological observations is the "sum" parameter Σ:

$$\Sigma = \sum_{i=1}^{3} m_i. \tag{15}$$

Moreover, the Jarlskog rephasing invariant quantity is given by [33]

$$J = s_x c_x s_y c_y s_z c_z^2 \sin\delta. \tag{16}$$

There are no experimental bounds on the phase angles, and we take the principal value range for δ, 2ρ and 2σ to be $[0, 2\pi]$. As to the other oscillation parameters, the experimental constraints give the values stated in Table I with 1, 2, and 3-σ errors [31,34]. Actually, the fits of oscillation data found in [31] and [34] are consistent with each other except that the latter fits are stricter for θ_z. In our numerical analysis, we prefer to use the former fit, which has a wider range for θ_z, in order to easily catch the pattern of variation depending on θ_z. Other groups [35,36] have also carried out global fits for the oscillation data and their findings are in line with those of the group of [31].

We adopt the less conservative 2-σ range as reported in [37] for the non oscillation parameters $\langle m \rangle_e$, Σ, whereas for the other nonoscillation parameter $\langle m \rangle_{ee}$ we use values found in [38]:

$$\begin{aligned} \langle m \rangle_e &< 1.8\ \mathrm{eV}, \\ \Sigma &< 1.19\ \mathrm{eV}, \\ \langle m \rangle_{ee} &< 0.34 - 0.78\ \mathrm{eV}. \end{aligned} \tag{17}$$

III. THE μ–τ SYMMETRY AND NEUTRINO MASS MATRIX

The μ–τ symmetry can be described by the following general set of conditions [22]:

$$|V_{\mu i}| = |V_{\tau i}|, \qquad \text{for } i = 1, 2, 3. \tag{18}$$

According to our adopted parametrizations for V in Eq. (2), these conditions imply two classes of solutions. The first class, hereafter labeled as class I, is characterized by

$$\theta_y = \frac{\pi}{4}, \qquad 2 s_x c_x s_z c_\delta = 0, \tag{19}$$

while the second class, hereafter labeled as class II, is determined by

$$\theta_z = \frac{\pi}{2}, \qquad s_{2x}s_{2y}c_\delta = c_{2y}c_{2x}. \tag{20}$$

The two classes, I and II, are distinguished by the possible allowed values for the mixing angles θ_y and θ_z. In class I, the mixing angle θ_y is fixed to be $\frac{\pi}{4}$, while for class II the mixing angle θ_z is fixed to be $\frac{\pi}{2}$. These restrictions are the only nontrivial consequence of the μ–τ symmetry. Regarding the other mixing angles and phases for each class, the restriction imposed through the symmetry is rather loose. However, according to the allowed values for mixing angles and phases, class II cannot be divided into a finite number of subclasses in contrast to class I, which can be divided into four subclasses as follows:

(a) $\theta_y = \frac{\pi}{4}$ and $\theta_x = 0$ while θ_z, δ, ρ and σ are free,
(b) $\theta_y = \frac{\pi}{4}$ and $\theta_x = \frac{\pi}{2}$ while θ_z, δ, ρ and σ are free,
(c) $\theta_y = \frac{\pi}{4}$ and $\theta_z = 0$ while θ_x, δ, ρ and σ are free,
(d) $\theta_y = \frac{\pi}{4}$ and $\delta = \pm\frac{\pi}{2}$ while θ_x, θ_z, ρ and σ are free.

The subclasses (a) and (b) seem unsatisfactory because the predicted θ_x is far from the experimentally preferred value. The remedy for this defect is to introduce a small perturbation having a large effect on θ_x, as was done in [22]. As to the subclass (c), it seems to be the most interesting class, from a phenomenological point of view, when joined with fixing θ_x near the experimentally preferred value. In a sense, it can contain models with tribimaximal, bimaximal, hexagonal, and A_5 symmetries. The last remaining subclass (d), predicting maximal CP violation, can include the tetramaximal symmetry [39]. Class II is phenomenologically disfavored since $\theta_z = \frac{\pi}{2}$ is far from the experimentally preferred value, which might justify dropping this whole class in the analysis carried out in [22].

We can get more insight into the μ–τ symmetry by writing its implications on the neutrino mass matrix entries. Class I and its subclasses are found to imply

(a) $M_{\nu 12} = M_{\nu 13}$ and $M_{\nu 22} = M_{\nu 33}$,
(b) $M_{\nu 12} = M_{\nu 13}$ and $M_{\nu 22} = M_{\nu 33}$,
(c) $M_{\nu 12} = -M_{\nu 13}$ and $M_{\nu 22} = M_{\nu 33}$,
(d) $M_{\nu 12} = M^*_{\nu 13}$ and $M_{\nu 22} = M^*_{\nu 33}$ for vanishing Majorana phases; otherwise no simple algebraic relation between the mass entries is found.

In the second class, II, the implied mass relations are

$$M_{\nu 12} = M_{\nu 13} = 0, \qquad \text{and} \qquad |M_{\nu 22}| = |M_{\nu 33}|. \tag{21}$$

The above mentioned considerations motivate us to take as a starting point one of the following mass relations as defining the μ–τ symmetry. The first relation is taken to be

$$M_{\nu 12} = M_{\nu 13}, \quad \text{and} \quad M_{\nu 22} = M_{\nu 33}, \tag{22}$$

while the second one is

$$M_{\nu 12} = -M_{\nu 13}, \qquad \text{and} \qquad M_{\nu 22} = M_{\nu 33}. \tag{23}$$

These two alternative ways for imposing μ–τ symmetry in Eq. (22) and Eq. (23) are respectively designated by S_+ and S_- in order to ease the corresponding referral. The other possible relations, like ($M_{\nu 12} = M^*_{\nu 13}$ and $M_{\nu 22} = M^*_{\nu 33}$) or ($M_{\nu 12} = M_{\nu 13} = 0$ and $|M_{\nu 22}| = |M_{\nu 33}|$), are disfavored because they involve a nonanalytical algebraic relation between mass entries that cannot be generated by the usual discrete flavor symmetries. There is still a further motivation for imposing μ–τ symmetry via S_+ or S_- that can be easily inferred from the symmetry properties enjoyed by the neutrino mass matrix as explained in Sec. II. In fact, the transformation rule in Eq. (6) singles out $\theta = \frac{\pi}{4}$ as a fixed point for the transformation and the mass relations in Eq. (7) already link the mass matrix entries relevant for the μ–τ symmetry. The difference in sign between the two alternative realizations, $M_{\nu 12} = \pm M_{\nu 13}$, can be attributed to the different phases assigned to the third neutrino field ν_τ.

IV. THE EXACT μ–τ SYMMETRY AS A TEXTURE FOR NONSINGULAR NEUTRINO MASS MATRIX

The exact μ–τ symmetry can be treated as a texture defined by

$$\begin{aligned} M_{\nu 12} \mp M_{\nu 13} &= 0, \\ M_{\nu 22} - M_{\nu 33} &= 0, \end{aligned} \tag{24}$$

where the minus and plus sign correspond respectively to the cases of Eq. (22) and Eq. (23).

Using Eqs. (2)–(4), the relation defining the texture can be expressed as

$$\begin{aligned} M_{\nu 12} \mp M_{\nu 13} = 0, &\Rightarrow \sum_{j=1}^{3} (U_{1j}U_{2j} \mp U_{1j}U_{3j})\lambda_j = 0 \\ &\Rightarrow A_1^\mp \lambda_1 + A_2^\mp \lambda_2 + A_3^\mp \lambda_3 = 0 \\ M_{\nu 22} - M_{\nu 33} = 0, &\Rightarrow \sum_{j=1}^{3} (U_{2j}U_{2j} - U_{3j}U_{3j})\lambda_j = 0, \\ &\Rightarrow B_1\lambda_1 + B_2\lambda_2 + B_3\lambda_3 = 0, \end{aligned} \tag{25}$$

where

$$A_j^\mp = U_{1j}(U_{2j} \mp U_{3j}), \qquad \text{and} \qquad B_j = U_{2j}^2 - U_{3j}^2, \quad (\text{no sum over } j). \tag{26}$$

The coefficients $A^\mp$ and B can be written explicitly in terms of mixing angles and the Dirac phase as

$$
\begin{aligned}
A_1^{\mp} &= -c_x c_z[c_x s_z(s_y \mp c_y) + s_x(c_y \pm s_y)e^{-i\delta}],\\
B_1 &= (c_x s_y s_z + s_x c_y e^{-i\delta})^2 - (-c_x c_y s_z + s_x s_y e^{-i\delta})^2,\\
A_2^{\mp} &= -s_x c_z[s_x s_z(s_y \mp c_y) \mp c_x(s_y \pm c_y)e^{-i\delta}],\\
B_2 &= (-s_x s_y s_z + c_x c_y e^{-i\delta})^2 - (s_x c_y s_z + c_x s_y e^{-i\delta})^2,\\
A_3^{\mp} &= s_z c_z(s_y \mp c_y),\\
B_3 &= c_z^2(s_y^2 - c_y^2).
\end{aligned} \tag{27}
$$

Provided λ_3 is nonvanishing, the equations (25) can be treated as two inhomogeneous linear equations of the ratios $\frac{\lambda_1}{\lambda_3}$ and $\frac{\lambda_2}{\lambda_3}$ that can be solved to get

$$
\begin{aligned}
\frac{\lambda_1}{\lambda_3} &= \frac{A_3^{\mp}B_2 - A_2^{\mp}B_3}{A_2^{\mp}B_1 - A_1^{\mp}B_2},\\
\frac{\lambda_2}{\lambda_3} &= \frac{A_1^{\mp}B_3 - A_3^{\mp}B_1}{A_2^{\mp}B_1 - A_1^{\mp}B_2}.
\end{aligned} \tag{28}
$$

Computing the mass spectrum, we find that it is always a degenerate one ($m_1 = m_2 = m_3$) leading to vanishing mass-squared differences, which is unacceptable phenomenologically. Explicitly, for the cases (a) to (c) mentioned in the previous section and respecting exact μ–τ symmetry, we have all the coefficients $A^{\mp}$s and Bs vanishing except $A_3^+ = -A_1^+ = s_z c_z$ (case a), $A_3^+ = -A_2^+ = s_z c_z$ (case b), and $A_1^- = -A_2^- = -\sqrt{2}s_x c_x e^{-i\delta}$ (case c).

V. THE EXACT μ–τ SYMMETRY AS A TEXTURE FOR SINGULAR NEUTRINO MASS MATRIX

One may wonder that our analysis might lead to nontrivial results for a singular neutrino mass matrix. Thus, it is crucial to carry the same study for the singular case, and keep in mind that the viable singular neutrino mass matrices have to be characterized by vanishing m_1 or m_3. The vanishing of m_2 leading to the simultaneous vanishing of m_1 and m_2 is not at all phenomenologically consistent.

A. Vanishing m_1 singular neutrino mass matrix having exact μ–τ symmetry

The mass spectrum in this case turns out to be

$$
\begin{aligned}
m_1 &= 0, \qquad m_2 = \sqrt{\delta m^2},\\
m_3 &= \sqrt{\Delta m^2 + \frac{\delta m^2}{2}} \approx \sqrt{\Delta m^2},
\end{aligned} \tag{29}
$$

which puts the mass ratio $\frac{m_2}{m_3}$ in the form

$$
m_{23} \equiv \frac{m_2}{m_3} = \sqrt{\frac{R_\nu}{1 + \frac{R_\nu}{2}}} \approx \sqrt{R_\nu}, \tag{30}
$$

where the phenomenologically acceptable value for R_ν is given in Table I. The vanishing of m_1 together with imposing the exact μ–τ symmetry as stated in Eqs. (25) leads to

$$
\begin{aligned}
A_2^{\mp}\lambda_2 + A_3^{\mp}\lambda_3 &= 0,\\
B_2\lambda_2 + B_3\lambda_3 &= 0,
\end{aligned} \tag{31}
$$

which gives nontrivial solutions, provided $A_2^{\mp}B_3 - A_3^{\mp}B_2 = 0$, i.e.,

$$
\begin{aligned}
m_{23} &= \left|\frac{A_3^{\mp}}{A_2^{\mp}}\right| = \left|\frac{B_3}{B_2}\right|,\\
\sigma &= \frac{1}{2}\mathrm{Arg}\left(-\frac{A_3^{\mp}m_3}{A_2^{\mp}m_2}\right) = \frac{1}{2}\mathrm{Arg}\left(-\frac{B_3 m_3}{B_2 m_2}\right).
\end{aligned} \tag{32}
$$

The Majorana phase ρ becomes unphysical, since m_1 vanishes, in this case, and can be dropped out.

These patterns can easily be shown to be unviable just by comparing the two approximate expressions obtained for $\frac{m_2}{m_3}$. As an example, we consider the case S_- where we have, as reported in Table II,

TABLE II. The approximate mass ratio formulas for the singular light neutrino mass realizing exact μ–τ symmetry. The formulas are calculated in terms of A's or B's coefficients.

Realization	$m_1 = 0$ $\frac{m_2}{m_3}$	
S_-	$\lvert\frac{A_3^-}{A_2^-}\rvert \approx \sqrt{\frac{1-s_{2y}}{1+s_{2y}}}\frac{s_z}{s_x c_x} + O(s_z^2)$	$\lvert\frac{B_3}{B_2}\rvert \approx \frac{1}{c_x^2}(1 + 2t_x t_{2y} c_\delta s_z) + O(s_z^2)$
S_+	$\lvert\frac{A_3^+}{A_2^+}\rvert \approx \sqrt{\frac{1+s_{2y}}{1-s_{2y}}}\frac{s_z}{s_x c_x} + O(s_z^2)$	$\lvert\frac{B_3}{B_2}\rvert \approx \frac{1}{c_x^2}(1 + 2t_x t_{2y} c_\delta s_z) + O(s_z^2)$
Realization	$m_3 = 0$ $\frac{m_2}{m_1}$	
S_-	$\lvert\frac{A_1^-}{A_2^-}\rvert \approx 1 - \frac{(1-s_{2y})c_\delta s_z}{c_{2y}s_x c_x} + O(s_z^2)$	$\lvert\frac{B_1}{B_2}\rvert \approx t_x^2(1 + \frac{2t_{2y}c_\delta s_z}{s_x c_x}) + O(s_z^2)$
S_+	$\lvert\frac{A_1^+}{A_2^+}\rvert \approx 1 + \frac{(1+s_{2y})c_\delta s_z}{c_{2y}s_x c_x} + O(s_z^2)$	$\lvert\frac{B_1}{B_2}\rvert \approx t_x^2(1 + \frac{2t_{2y}c_\delta s_z}{s_x c_x}) + O(s_z^2)$

$$m_{23} \approx \begin{cases} \sqrt{\frac{1-s_{2y}}{1+s_{2y}}}\frac{s_z}{s_x c_x} + O(s_z^2), & \text{from A}^-\text{s}, \\ \frac{1}{c_x^2}(1 + 2t_x t_{2y} c_\delta s_z) + O(s_z^2), & \text{from Bs}. \end{cases} \quad (33)$$

This mass ratio, $\frac{m_2}{m_3}$, should be consistent with the constraint of Eq. (30), which means that it should be much less than one. It is hard to satisfy this constraint because the first expression, obtained from A^-s, starts from $O(s_z)$ and can be tuned to a small value, while the second one, obtained from Bs, has a leading contribution ($\frac{1}{c_x^2}$) that is greater than one for the admissible range of θ_x. To properly tune the second expression, one needs large negative higher order corrections that can be achieved by choosing negative c_δ and letting θ_y approach $\frac{\pi}{4}$, but this tends in its turn to diminish the first expression of the mass ratio more than required. Thus, the two expressions cannot be made compatible. A similar reasoning can be applied to the case S_+ to show the incompatibility of the two derived expressions for the mass ratio. Our numerical study confirms this conclusion where all the phenomenologically acceptable ranges for mixing angles and the Dirac phase are scanned, but no solutions could be found satisfying the mass constraint expressed in Eq. (30).

B. The vanishing m_3 singular neutrino mass matrix having exact μ–τ symmetry

Along the same lines as the previous subsection, we can treat the case of vanishing m_3. This time, the mass spectrum is found to be

$$m_1 = \sqrt{\Delta m^2 - \frac{\delta m^2}{2}}, \qquad m_2 = \sqrt{\Delta m^2 + \frac{\delta m^2}{2}}, \qquad m_3 = 0, \quad (34)$$

forcing the mass ratio $\frac{m_2}{m_1}$ to be

$$m_{21} \equiv \frac{m_2}{m_1} = \sqrt{\frac{1+\frac{R_\nu}{2}}{1-\frac{R_\nu}{2}}} \approx 1 + \frac{R_\nu}{2} \gtrsim 1. \quad (35)$$

The vanishing of m_3 together with imposing exact μ–τ symmetry as stated in Eqs. (25) results in the following equations:

$$A_1^\mp \lambda_1 + A_2^\mp \lambda_2 = 0, \qquad B_1 \lambda_1 + B_2 \lambda_2 = 0, \quad (36)$$

which have nontrivial solutions of

$$m_{21} = \left|\frac{A_1^\mp}{A_2^\mp}\right| = \left|\frac{B_1}{B_2}\right|, \qquad \rho - \sigma = \frac{1}{2}\mathrm{Arg}\left(-\frac{A_2^\mp m_2}{A_1^\mp m_1}\right) = \frac{1}{2}\mathrm{Arg}\left(-\frac{B_2 m_2}{B_1 m_1}\right), \quad (37)$$

provided $A_1^\mp B_2 - A_2^\mp B_1 = 0$. It is clear that the only relevant physical combination of Majorana phases in such a case is the difference $\rho - \sigma$. One can use the same reasoning explained in the case of vanishing m_1, based on approximate formulas for mass ratios, as reported in Table II, to show that the constraint of Eq. (35) cannot be satisfied, which makes the patterns unviable. Again, our numerical study based on scanning all phenomenologically acceptable ranges for mixing angles and the Dirac phase reveals no found solutions satisfying the constraint of Eq. (35).

Our investigations, which are so far model independent, point out that imposing exact μ–τ symmetry always produces phenomenologically unsatisfactory results. Thus, one might find solace by demanding violation of the exact μ–τ symmetry. In breaking the symmetry, we are going to try the simplest and the minimal ways of breaking.

VI. DEVIATION FROM EXACT μ–τ SYMMETRY

We consider the simplest minimal possible deviation from the exact μ–τ symmetry that can be parametrized by only one parameter. The relations characterizing these deviations can assume the following two forms:

$$M_{\nu 12}(1+\chi) = \pm M_{\nu 13}, \quad \text{and} \quad M_{\nu 22} = M_{\nu 33}, \quad (38)$$

and

$$M_{\nu 12} = \pm M_{\nu 13}, \quad \text{and} \quad M_{\nu 22}(1+\chi) = M_{\nu 33}, \quad (39)$$

where $\chi = |\chi| e^{i\theta}$ is a complex parameter measuring the deviation from exact μ–τ symmetry. The absolute value $|\chi|$ is restricted to fall in the range [0,0.2], while the phase θ is totally free. The chosen range for χ is made to ensure a small deviation that can be treated as a perturbation.

The deviation from exact μ–τ symmetry can be treated in an illuminating way by considering the relations in Eqs. (38) and (39) as defining the following textures:

$$M_{\nu 12}(1+\chi) \mp M_{\nu 13} = 0, \quad \text{and} \quad M_{\nu 22} - M_{\nu 33} = 0, \quad (40)$$

and

$$M_{\nu 12} \mp M_{\nu 13} = 0, \quad \text{and} \quad M_{\nu 22}(1+\chi) - M_{\nu 33} = 0. \quad (41)$$

Following the same procedure as described in Sec. IV, we find that the coefficients As and Bs corresponding to the textures defined in Eq. (40) and Eq. (41) are, respectively,

$$A_j^\mp = U_{1j}[U_{2j}(1+\chi) \mp U_{3j}], \quad \text{and} \quad B_j = U_{2j}^2 - U_{3j}^2, \quad (\text{no sum over } j) \quad (42)$$

and

$$A_j^{\mp} = U_{1j}(U_{2j} \mp U_{3j}), \qquad \text{and}$$
$$B_j = U_{2j}^2(1+\chi) - U_{3j}^2, \qquad (\text{no sum over } j). \tag{43}$$

Assuming $\lambda_3 \neq 0$, the resulting λ's ratio are found to be

$$\frac{\lambda_1}{\lambda_3} = \frac{A_3B_2 - A_2B_3}{A_2B_1 - A_1B_2},$$
$$\frac{\lambda_2}{\lambda_3} = \frac{A_1B_3 - A_3B_1}{A_2B_1 - A_1B_2}. \tag{44}$$

From these λ ratios, the mass ratios $(\frac{m_1}{m_3}, \frac{m_2}{m_3})$ and Majorana phases (ρ, σ) can be determined in terms of the mixing angles $(\theta_x, \theta_y, \theta_z)$, the Dirac phase δ, and the complex parameter χ. Thus, we can vary $(\theta_x, \theta_y, \theta_z, \delta m^2)$ over their experimentally allowed regions and $(\delta, |\chi|, \theta)$ in their full range to determine the unknown mass spectra and Majorana phases. We can then confront the whole predictions with the experimental constraints given in Table I and Eq. (17) to find out the admissible seven-dimensional parameter space region. For a proper survey of the allowed parameter space, one can illustrate graphically all the possible correlations, at the three levels of σ error, between any two physical neutrino parameters. We chose to plot for each pattern and for each type of hierarchy thirty-four correlations at the 3-σ error level involving the parameters $(m_1, m_2, m_3, \theta_x, \theta_y, \theta_z, \rho, \sigma, \delta, J, m_{ee}, |\chi|, \theta)$ and the lowest neutrino mass (LNM). Moreover, for each parameter, one can determine the extremum values it can take according to the considered precision level, and we listed in tables these predictions for all the patterns and for the three σ-error levels.

The resulting mass patterns are found to be classifiable into three categories:

(i) Normal hierarchy: characterized by $m_1 < m_2 < m_3$ and denoted by **N** satisfying numerically the bound

$$\frac{m_1}{m_3} < \frac{m_2}{m_3} < 0.7, \tag{45}$$

(ii) Inverted hierarchy: characterized by $m_3 < m_1 < m_2$ and denoted by **I** satisfying the bound

$$\frac{m_2}{m_3} > \frac{m_1}{m_3} > 1.3, \tag{46}$$

(iii) Degenerate hierarchy (meaning quasidegeneracy): characterized by $m_1 \approx m_2 \approx m_3$ and denoted by **D**. The corresponding numeric bound is taken to be

$$0.7 < \frac{m_1}{m_3} < \frac{m_2}{m_3} < 1.3. \tag{47}$$

Moreover, we studied for each pattern the possibility of having a singular (noninvertible) mass matrix characterized by one of the masses (m_1 and m_3) being equal to zero (the data prohibits the simultaneous vanishing of two masses and thus m_2 cannot vanish).

VII. NUMERICAL RESULTS OF VARIOUS PATTERNS VIOLATING EXACT μ–τ SYMMETRY

We now present the results of our numerical analysis for the four simplest possible patterns violating exact μ–τ as described in the previous section and quantified in Eq. (40) and Eq. (41). The coefficients' As and Bs are expressed in Eq. (42) and Eq. (43) according to the pattern under study. Moreover, analytical expressions of the relevant parameters up to the leading order in s_z are provided in order to get an "understanding" of the numerical results. The relevant parameters include mass ratios, Majorana phases, the R_ν parameter, the effective Majorana mass term $\langle m \rangle_{ee}$, and the effective electron's neutrino mass $\langle m \rangle_e$. We stress here that our numerical analysis is based on the exact formulas and not on the approximate ones.

The large number of correlation figures is organized in plots, at the 3-σ error level, by dividing each figure into left and right panels (halves) denoted accordingly by the letters L and R. Additional labels (D, N, and I) are attached to the plots to indicate the type of hierarchy (degenerate, normal, and inverted, respectively). Any missing label D, N, or I on the figures of a certain pattern means the absence of the corresponding hierarchy type in this pattern.

We list in tables III and IV, and for the three types of hierarchy and the three precision levels, the extremum values that the different parameters can take. It is noteworthy that our numerical study is based, as was the case in [32], on random scanning of the seven-dimensional parameter space composed of (θ_x, θ_y, θ_z, δ, δm^2, $|\chi|$ and θ). This kind of randomness implies that the reported values in the tables are meant to give only a strong qualitative indication, in that they might change from one run to another, thus providing a way to check for the stability of the results.

A. C1: Pattern having $M_{\nu 12}(1+\chi) - M_{\nu 13} = 0$, and $M_{\nu 22} - M_{\nu 33} = 0$

In this pattern, C1, the relevant expressions for As and Bs are

$$\begin{aligned}
A_1 &= -c_x c_z(c_x s_y s_z + s_x c_y e^{-i\delta})(1+\chi) \\
&\quad - c_x c_z(-c_x c_y s_z + s_x s_y e^{-i\delta}), \\
A_2 &= s_x c_z(-s_x s_y s_z + c_x c_y e^{-i\delta})(1+\chi) \\
&\quad + s_x c_z(s_x c_y s_z + c_x s_y e^{-i\delta}), \\
A_3 &= s_z s_y c_z(1+\chi) - s_z c_y c_z, \\
B_1 &= (c_x s_y s_z + s_x c_y e^{-i\delta})^2 - (-c_x c_y s_z + s_x s_y e^{-i\delta})^2, \\
B_2 &= (-s_x s_y s_z + c_x c_y e^{-i\delta})^2 - (s_x c_y s_z + c_x s_y e^{-i\delta})^2, \\
B_3 &= s_y^2 c_z^2 - c_y^2 c_z^2,
\end{aligned} \tag{48}$$

TABLE III. The various prediction for the patterns of violating exact μ–τ symmetry. All the angles (masses) are evaluated in degrees (eV).

Pattern: $M_{\nu 12}(1+\chi) - M_{\nu 13} = 0$, and $M_{\nu 22} - M_{\nu 33} = 0$												
quantity	θ_x	θ_y	θ_z	m_1	m_2	m_3	ρ	σ	δ	$\langle m \rangle_e$	$\langle m \rangle_{ee}$	J
						Degenerate Hierarchy						
1σ	32.96 – 35.00	38.77 – 44.99	7.71–10.30	0.0470–0.3975	0.0478–0.3976	0.0583–0.3971	0.1910–177.00	0.1915–176.96	[0.3653 – 176.6]∪[180.8 – 358.27]	0.0479–0.3975	0.0448–0.3939	−0.0402 – 0.0402
2σ	31.95–36.09	36.88–50.77	6.29–11.68	0.0463–0.3942	0.0471–0.3943	0.0568–0.3970	0.2341–178.17	0.2670–178.16	[0.7333 – 173.3]∪[180.3 – 357.99]	0.0470–0.3942	0.0429–0.3938	−0.0459 – 0.0444
3σ	30.98–37.11	36.96–52.01	4.08–12.92	0.0457–0.3947	0.0465–0.3948	0.0557–0.3975	0.1981–179.55	0.2046–179.46	[0.1882 – 176.7]∪[180.6 – 359.79]	0.0463–0.3949	0.0411–0.3947	−0.0502 – 0.0506
						Normal Hierarchy						
1σ	32.96–35.00	44.29–44.96	7.71–10.30	0.0163–0.0471	0.0186–0.0479	0.0510–0.0686	9.71–167.30	9.77–167.1	[14.44 – 167.1]∪[188 – 354.00]	0.019–0.0481	0.0151–0.0476	[−0.0406 – −0.0041]∪[0.0079 – 0.0404]
2σ	31.95–36.09	[44.03 – 44.95]∪[45.05 – 46.07]	6.29–11.68	0.0129–0.0483	0.0155–0.0491	0.0497–0.0703	7.36–171.71	7.32–171.56	[3.22 – 166.9]∪[188.2 – 346.46]	0.0166–0.0496	0.0115–0.0485	[−0.0456 – −0.0061]∪[0.0021 – 0.0457]
3σ	30.98–37.10	[43.87 – 44.98]∪[45.04 – 46.30]	4.11–12.92	0.0124–0.0490	0.0151–0.0498	0.0485–0.0714	4.48–175.92	4.88–175.83	[8.71 – 173.5]∪[190.1 – 357.69]	0.0168–0.050	0.0107–0.0496	[−0.0504 – −0.0019]∪[0.0053 – 0.050]
						Inverted Hierarchy						
1σ	32.96–35.00	43.89–44.97	7.71–10.30	0.0463–0.0783	0.0471–0.0787	7.4×10^{-4} −0.0602	0.2721–179.84	0.0356–179.49	[2.87 – 117.4]∪[235.6 – 357.6]	0.0459–0.0779	0.0452–0.0779	[−0.0403 – −0.0017]∪[0.0020 – 0.0402]
2σ	31.95–36.08	[43.57 – 44.97]∪[45.04 – 46.13]	6.29–11.68	0.0466–0.0783	0.0474–0.0788	8.48×10^{-4} −0.0601	0.0617–179.40	0.0771–179.81	[7.11 – 174.1]∪[185.7 – 356.34]	0.0461–0.0780	0.0453–0.0775	[−0.0453 – −0.0020]∪[0.0033 – 0.0456]
3σ	30.98–37.11	[43.46 – 44.98]∪[45.02 – 46.35]	4.05–12.92	0.0452–0.0802	0.0460–0.0806	3.2×10^{-4} −0.0617	0.8583–179.39	0.5892–179.73	[6.60 – 172.4]∪[188.7 – 352.83]	0.0445–0.0796	0.0436–0.0784	[−0.0501 – −0.0036]∪[0.0036 – 0.0504]
Pattern $M_{\nu 12}(1+\chi) + M_{\nu 13} = 0$, and $M_{\nu 22} - M_{\nu 33} = 0$												
quantity	θ_x	θ_y	θ_z	m_1	m_2	m_3	ρ	σ	δ	$\langle m \rangle_e$	$\langle m \rangle_{ee}$	J
						Degenerate Hierarchy						
1σ	32.96–35.00	38.65–45.91	7.71–10.30	0.0475–0.3950	0.0483–0.3951	0.0579–0.3979	[0.1509 – 40.42]∪[136.9 – 179.95]	0.5750–179.29	[2.83 – 164.7]∪[199.5 – 356.94]	0.0482–0.3950	0.0193–0.3947	−0.0396 – 0.0406
2σ	31.95–36.10	36.87–50.77	6.29–11.68	0.0471–0.3959	0.0479–0.3960	0.0579–0.3927	[0.0045 – 88.53]∪[111.5 – 179.95]	0.5585–179.45	[1.96 – 174.7]∪[189.9 – 352.1]	0.0477–0.3958	0.0155–0.3958	[−0.0453 – −0.004]∪[0.001 – 0.0448]
3σ	30.98–37.11	35.67–53.10	4.05–12.92	0.0454–0.3947	0.0462–0.3948	0.0554–0.3980	[0.0064 – 93.2]∪[99.53 – 179.90]	0.6741–179.36	[4.71 – 167.8]∪[188 – 350.9698]	0.0459–0.3949	0.0148–0.3941	[−0.0496 – −0.0034]∪[0.0019 – 0.0492]
						Normal Hierarchy						
1σ	32.98–34.99	40.85–42.05	7.71–8.16	0.0444–0.0474	0.0452–0.0482	0.0655–0.0689	[5.01 – 23.17]∪[156.9 – 177.81]	[41.78 – 74.46]∪[100.3 – 137.8190]	[15.28 – 78.84]∪[279 – 352.81]	0.0451–0.0481	0.0175–0.0298	[−0.0304 – −0.0123]∪[0.008 – 0.0302]
2σ	31.95–36.09	[40.70 – 43.12]∪[46.45 – 50.31]	6.29–9.89	0.0345–0.0485	0.0356–0.0493	0.0586–0.0704	[0.1354 – 59.76]∪[121.2 – 179.89]	18.58–162.63	[12.42 – 177.6]∪[185.9 – 345.12]	0.0353–0.0493	0.0120–0.0406	[−0.0346 – −0.003]∪[0.005 – 0.0371]
3σ	30.98–37.11	[40.88 – 44.26]∪[45.52 – 50.43]	4.05–9.87	0.0246–0.0495	0.0260–0.0502	0.0521–0.0718	[0.0144 – 89.4]∪[112.4 – 179.44]	4.49–173.68	[10.79 – 167.3]∪[187.6 – 353.32]	0.0253–0.0500	0.0067–0.0453	[−0.0374 – −0.0024]∪[0.0045 – 0.0347]
						Inverted Hierarchy						
1σ	32.96–35.00	38.65–43.46	7.71–10.30	0.0551–0.0784	0.0558–0.0789	0.0294–0.0603	[3.54 – 19.71]∪[160.2 – 176.77]	[14.78 – 69.1]∪[109.7165.11]	[18.51 – 121.2]∪[236.7 – 343.59]	0.0550–0.0781	0.0289–0.0717	[−0.0400 – −0.01]∪[0.01 – 0.0398]
2σ	31.95–36.09	[36.89 – 43.81]∪[46.3 – 50.77]	6.29–11.67	0.0526–0.0784	0.0534–0.0788	0.0248–0.0602	[0.4268 – 28.53]∪[153.5 – 177.64]	9.58–168.19	[6.25 – 157.6]∪[196.6 – 347.4449]	0.0526–0.0779	0.0199–0.0724	[−0.0439 – −0.007]∪[0.003 – 0.0438]
3σ	30.98–37.11	[35.7 – 44.39]∪[45.57 – 53.13]	4.05–12.84	0.0468–0.0797	0.0476–0.0802	0.0118–0.0612	[0.1457 – 48.96]∪[137.7 – 179.93]	4.47–170.68	[4.56 – 162.9]∪[190.2 – 341.24]	0.0469–0.0798	0.0145–0.0730	[−0.0488 – −0.0038]∪[0.0019 – 0.0470]

(Table continued)

TABLE III. (*Continued*)

Pattern: $M_{\nu 12}(1+\chi) - M_{\nu 13} = 0$, and $M_{\nu 22} - M_{\nu 33} = 0$												
Pattern: $M_{\nu 12} - M_{\nu 13} = 0$, and $M_{\nu 22}(1+\chi) - M_{\nu 33} = 0$												
quantity	θ_x	θ_y	θ_z	m_1	m_2	m_3	ρ	σ	δ	$\langle m \rangle_e$	$\langle m \rangle_{ee}$	J
						Degenerate Hierarchy						
1σ	32.96 – 35	38.65–44.848	7.71–10.30	0.0472–0.3790	0.0480–0.3791	0.0579–0.3822	0.0149–179.30	0.0169–179.29	0.0484–359.94	0.0480–0.3791	0.0447–0.3718	−0.0398 – 0.0398
2σ	31.95–36.09	[36.87 – 44.88]∪ [45.13 – 50.77]	6.29–11.68	0.0465–0.3951	0.0473–0.3952	0.0574–0.3921	0.0305–179.84	0.0546–179.84	0.0702–359.88	0.0472–0.3950	0.0435–0.3949	−0.0442 – 0.0447
3σ	30.98–37.11	[35.67 – 44.93]∪ [45.08 – 53.1295]	4.06–12.92	0.0453–0.3777	0.0462–0.3778	0.0556–0.3810	0.0191 – 180	0.0192 – 180	0.0257–359.86	0.0463–0.3779	0.0421–0.3761	−0.0488 – 0.0487
						Normal Hierarchy						
1σ	32.96 – 35	38.65–43.72	7.72–10.30	0.0259–0.0473	0.0272–0.0481	0.0550–0.0689	0.2156–179.98	0.0009–179.97	[0.1287 – 172.7]∪ [193.3 – 359.1856]	0.0277–0.0481	0.0256–0.0479	−0.0393 – 0.0399
2σ	31.95–36.09	[36.88 – 44.04]∪ [46.1 – 50.77]	6.30–11.68	0.0223–0.0481	0.0239–0.0489	0.0531–0.0701	0.0070–179.98	0.0522–179.95	[0.0141 – 171.5]∪ [181.7 – 359.94]	0.0247–0.0493	0.0216–0.0490	−0.0452 – 0.0456
3σ	30.98–37.11	[35.67 – 43.87]∪ [46.17 – 53.12]	4.08–12.92	0.0198–0.0492	0.0216–0.0500	0.0503–0.0715	0.0615 – 180	0.0269–179.99	0.1590–359.92	0.0228–0.0503	0.0199–0.0498	−0.0493 – 0.0492
						Inverted Hierarchy						
1σ	32.96–35.00	38.65–44.36	7.71–10.30	0.0464–0.0776	0.0472–0.0781	0.0008–0.0592	0.0224–179.77	0.0452–179.73	59.89–281.52	0.0461–0.0774	0.0455–0.0773	−0.0390 – 0.0396
2σ	31.95–36.09	[36.89 – 44.32]∪ [45.64 – 50.77]	6.30–11.68	0.0463–0.0777	0.0471–0.0782	0.0019–0.0598	0.1213–179.93	0.0469–179.96	0.1177–359.95	0.0458–0.0776	0.0448–0.0775	−0.0439 – 0.0445
3σ	30.98–37.10	[35.70 – 44.48]∪ [45.63 – 53.13]	4.05–12.92	0.0453–0.0790	0.0462–0.0794	0.0006–0.0604	0.0132–179.99	0.0244–179.84	0.0079–359.91	0.0448–0.0788	0.0436–0.0782	−0.0486 – 0.0492
Pattern: $M_{\nu 12} + M_{\nu 13} = 0$, and $M_{\nu 22}(1+\chi) - M_{\nu 33} = 0$												
quantity	θ_x	θ_y	θ_z	m_1	m_2	m_3	ρ	σ	δ	$\langle m \rangle_e$	$\langle m \rangle_{ee}$	J
						Degenerate Hierarchy						
1σ	32.96 – 35	38.65–44.98	7.71–10.30	0.0757–0.3966	0.0755–0.3965	0.0293–0.3962	[0.0844 – 40.68]∪ [135.6 – 179.67]	1.29–177.65	0.2316–359.73	0.0745–0.3954	0.0483–0.3617	−0.0397 – 0.0395
2σ	31.95–36.09	36.87–50.77	6.29–11.68	0.0658–0.3955	0.0664–0.3956	0.0574–0.3926	[0.0111 – 63.82]∪ [113 – 179.59]	1.38–176.99	0.4530–359.73	0.0663–0.3955	0.0231–0.3628	−0.0446 – 0.0443
3σ	30.99–37.10	35.67–53.13	4.05–12.90	0.0456–0.3902	0.0464–0.3903	0.0561–0.3875	0.1229–179.71	0.1735–177.30	0.4436–359.90	0.0460–0.3902	0.0138–0.3377	−0.0474 – 0.0484
						Normal Hierarchy						
1σ	×	×	×	×	×	×	×	×	×	×	×	×
2σ	×	×	×	×	×	×	×	×	×	×	×	×
3σ	30.99–37.11	[35.68 – 37.61]∪ [50.89 – 53.13]	4.05–4.67	0.0378–0.0493	0.0388–0.0501	0.0595–0.0717	20.85–156.35	0.3957–178.58	[0.7022 – 158]∪ [188.4 – 358.43]	0.0383–0.0497	0.0104–0.0297	−0.0179 – 0.0176
						Inverted Hierarchy						
1σ	×	×	×	×	×	×	×	×	×	×	×	×
2σ	31.95–36.09	36.87–50.77	6.29–8.07	0.0652–0.0787	0.0657–0.0792	0.0458–0.0605	[0.1822 – 90.22]∪ [94.89 – 178.27]	0.0532–179.63	0.1149–354.39	0.0651–0.0787	0.0203–0.0635	−0.0291 – 0.0295
3σ	30.98–37.11	35.68–53.12	4.05–7.73	0.0554–0.0795	0.0561–0.0800	0.0314–0.0611	0.1136–179.52	0.0084–179.96	0.2029–359.92	0.0555–0.0796	0.0175–0.0725	−0.0274 – 0.0295

TABLE IV. The allowed values for $|\chi|$ (pure number) and θ for the patterns of violating exact μ–τ symmetry. All the angles are evaluated in degrees.

Pattern : $M_{\nu 12}(1+\chi) - M_{\nu 13} = 0$, and $M_{\nu 22} - M_{\nu 33} = 0$					
$\lvert\chi\rvert$			θ		
1σ	2σ	3σ	1σ	2σ	3σ
Degenerate Hierarchy					
0.0023–0.2	0.0030–0.2	0.0047–0.2	0.85–359.6	0.75–359.12	0.82–359.2
Normal Hierarchy					
0.0398–0.2	0.0434–0.2	0.0378–0.2	[3.43 – 91]∪[269.9 – 351.77]	[11.74 – 90.57]∪[101 – 172.5]∪ [188.4 – 263.4]∪[277.5 – 358.13]	[8.73 – 89.7]∪[104 – 176]∪ [186 – 262]∪[273.5 – 352.6]
Inverted Hierarchy					
0.0309–0.2	0.020–0.2	0.0276–0.2	[13.51 – 1272.2]∪[188.1 – 349.7]	[8.48 – 172.9]∪[188 – 349]	[8.55 – 172.7]∪[185.8 – 350.3]
Pattern : $M_{\nu 12}(1+\chi) + M_{\nu 13} = 0$, and $M_{\nu 22} - M_{\nu 33} = 0$					
$\lvert\chi\rvert$			θ		
1σ	2σ	3σ	1σ	2σ	3σ
Degenerate Hierarchy					
0.0066–0.2	0.0085–0.2	0.0049–0.2	[0.075 – 50.24]∪[59.11 – 77.88]∪ [129.4 – 233.3]∪[288.4 – 359.9]	[0.20 – 76.48]∪[108.4 – 242.2]∪ [300.8 – 359.78]	[0.1 – 70.91]∪[85.6 – 254.1]∪ [276.5 – 359.74]
Normal Hierarchy					
0.1889–0.2	0.14–0.2	0.1–0.2	[0.48 – 2.17]∪[357.7 – 359.8]	[0.43 – 3.1]∪[176.7 – 183.4]∪ [356.5 – 359.54]	[0.33 – 4.9]∪[173.2 – 185]∪ [355.1 – 359.75]
Inverted Hierarchy					
0.0992–0.2	0.0814–0.2	0.06–0.2	[176.08 – 179.6]∪[180.4 – 184.12]	[0.57 – 4.98]∪[175.6 – 184.4]∪ [355.6 – 359.65]	[0.33 – 6.6]∪[174.3 – 186.8]∪ [353.8 – 359.87]
Pattern : $M_{\nu 12} - M_{\nu 13} = 0$, and $M_{\nu 22}(1+\chi) - M_{\nu 33} = 0$					
$\lvert\chi\rvert$			θ		
1σ	2σ	3σ	1σ	2σ	3σ
Degenerate Hierarchy					
0.0017–0.2	0.0016–0.2	0.0025–0.2	0.30–359.75	0.08–359.84	0.15–359.65
Normal Hierarchy					
0.0729–0.2	0.0658–0.2	0.0587–0.2	[0.17 – 74.5]∪[285.6 – 359.12]	[0.40 – 74.9]∪[114.3 – 247.4]∪ [286.3 – 359.68]	[0.08 – 72.7]∪[112.4 – 246.9]∪ [285.4 – 359.54]
Inverted Hierarchy					
0.0393–0.2	0.0345–0.2	0.0426–0.2	110.1–251.33	[0.13 – 77.84]∪[112.5 – 250.5]∪ [283.3 – 359.87]	[0.21 – 76.57]∪[108.3 – 247.6]∪ [283.7 – 359.87]
Pattern : $M_{\nu 12} + M_{\nu 13} = 0$, and $M_{\nu 22}(1+\chi) - M_{\nu 33} = 0$					
$\lvert\chi\rvert$			θ		
1σ	2σ	3σ	1σ	2σ	3σ
Degenerate Hierarchy					
0.0112–0.2	0.0079–0.2	0.0115–0.2	1.53–359.94	0.61–358.42	0.82–359.45
Normal Hierarchy					
×	×	0.16–0.2	×	×	[0.12 – 19.47]∪[139.9 – 217.4]∪ [340.8 – 359.9]
Inverted Hierarchy					
×	0.1572–0.2	0.1047–0.2	×	45.7–310.22	0.03 – 360

leading to mass ratios, up to the leading order in s_z, of

$$m_{13} \equiv \frac{m_1}{m_3} \approx 1 + \frac{2 s_\delta s_\theta |\chi| s_z}{t_x T_1},$$
$$m_{23} \equiv \frac{m_2}{m_3} \approx 1 - \frac{2 t_x s_\delta s_\theta |\chi| s_z}{T_1}, \tag{49}$$

where T_1 is defined as

$$T_1 = |\chi|^2 c_y^2 + 2|\chi| c_\theta c_y (c_y + s_y) + 1 + s_{2y} \tag{50}$$

while the Majorana phases are

$$\rho \approx \delta + \frac{s_\delta s_z (-s_y c_y |\chi|^2 + |\chi| c_\theta (c_{2y} - s_{2y}) + c_{2y})}{t_x T_1},$$
$$\sigma \approx \delta - \frac{s_\delta t_x s_z (-s_y c_y |\chi|^2 + |\chi| c_\theta (c_{2y} - s_{2y}) + c_{2y})}{T_1}. \tag{51}$$

The parameters R_ν, the mass ratio square difference $m_{23}^2 - m_{13}^2$, $\langle m \rangle_e$ and $\langle m \rangle_{ee}$, can be deduced to be

$$R_\nu \approx -\frac{8 s_\delta s_\theta |\chi| s_z}{s_{2x} T_1},$$
$$m_{23}^2 - m_{13}^2 \approx -\frac{8 s_\delta s_\theta |\chi| s_z}{s_{2x} T_1},$$
$$\langle m \rangle_e \approx m_3 \left[1 + \frac{4 s_\theta s_\delta |\chi| s_z}{t_{2x} T_1}\right],$$
$$\langle m \rangle_{ee} \approx m_3 \left[1 + \frac{4 s_\theta s_\delta |\chi| s_z}{t_{2x} T_1}\right]. \tag{52}$$

Our expansion in terms of s_z is justified since s_z is typically small for phenomenologically acceptable values where the best fit for $s_z \approx 0.144$. Therefore, we naively expect that the expansion should work properly but it turns out that there are

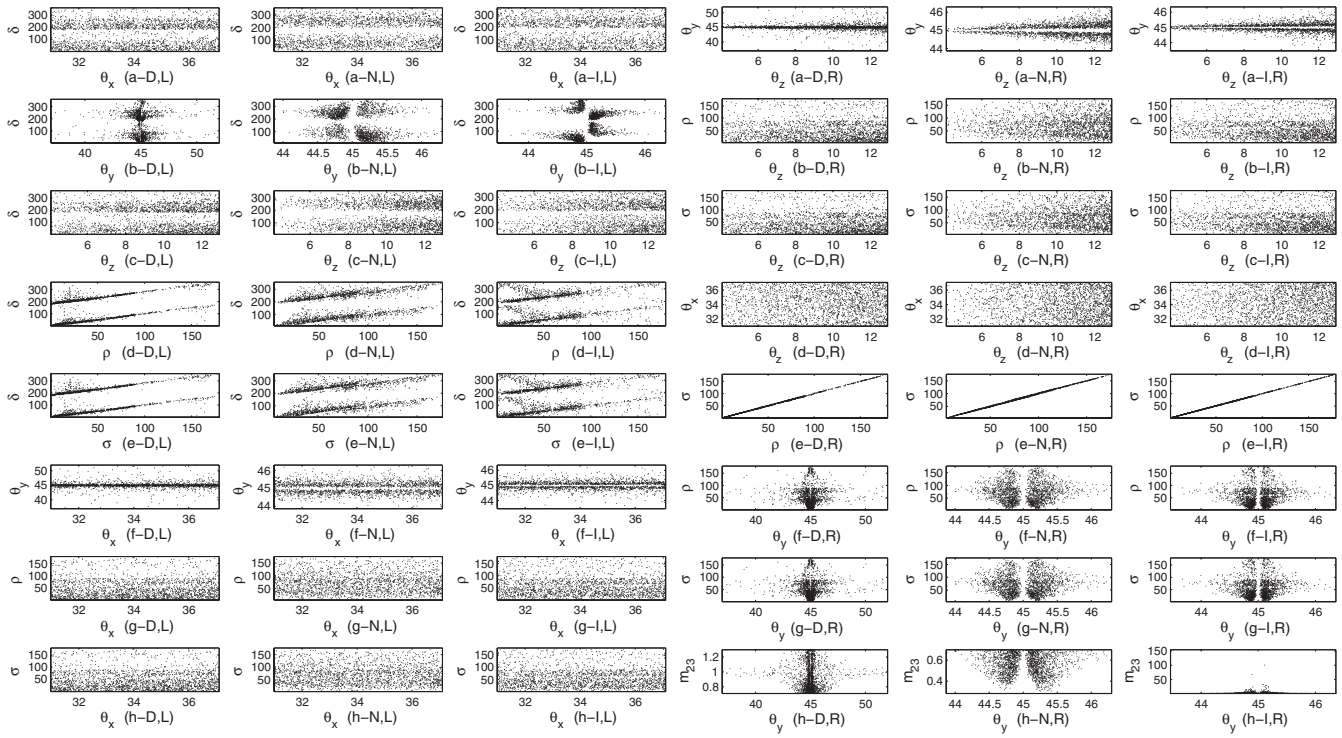

FIG. 1. Pattern having $M_{\nu 12}(1+\chi) - M_{\nu 13} = 0$, and $M_{\nu 22} - M_{\nu 33} = 0$. The left panel (the left three columns) presents correlations of δ against mixing angles and Majorana phases (ρ and σ) and those of θ_x against θ_y, ρ, and σ. The right panel (the right three columns) shows the correlations of θ_z against θ_y, ρ, σ, and θ_x and those of ρ against σ and θ_y, and also the correlation of θ_y versus σ and m_{23}.

some subtle points in this expansion which would invalidate our naive expectation. To elaborate on this, let us consider the expansion corresponding to the mass ratio m_{13} as

$$m_{13} = 1 + \sum_{i=1}^{\infty} c_i(\theta_x, \theta_y, \delta, |\chi|, \theta) s_z^i, \tag{53}$$

where c_i is the ith-Taylor expansion coefficient depending on $\theta_x, \theta_y, \delta, |\chi|$, and θ. In this pattern, putting θ_y equal to $\frac{\pi}{4}$ makes the spectrum degenerate $(m_{13} = m_{23} = 1)$ irrespective of the values for $\theta_x, \delta, |\chi|$ and θ. There are two possible alternatives to match this finding: in the first one, all the $c_i(\theta_y = \frac{\pi}{4})$s are vanishing, whereas in the second one some of the $c_i(\theta_y = \frac{\pi}{4})$s are finite and nonvanishing provided that an infinite number of $c_i(\theta_y = \frac{\pi}{4})$s are divergent such that the coefficients recombine in a delicate way to make the sum $\sum_{i=1}^{\infty} c_i(\theta_x, \theta_y = \frac{\pi}{4}, \delta, |\chi|, \theta) s_z^i$ equaling zero for any s_z.[1]

Explicit calculation reveals that c_1 is finite and nonvanishing at $\theta_y = \frac{\pi}{4}$ as is evident from Eq. (49), while c_i is divergent at $\theta_y = \frac{\pi}{4}$ for all $i \geq 2$. A similar consideration applies also to the mass ratio m_{23}. These divergences, at $\theta_y = \frac{\pi}{4}$, appearing in the expansion coefficients c_i for mass ratios resurface again in the expansion coefficients corresponding to $\langle m \rangle_e$ and $\langle m \rangle_{ee}$ but surprisingly enough the divergences associated with R_ν and $m_{23}^2 - m_{13}^2$ start only from the third order coefficients. All these subtleties are an artifact of the expansion, whereas no such problems arise if we use exact formulas. Thus, the formulas due to expansion must be dealt with with caution.

All the possible fifteen pair correlations related to the three mixing angles and the three Majorana and the Dirac phases $(\theta_x, \theta_y, \theta_z, \delta, \rho, \sigma)$ are presented in the left and right panels of Fig. 1, while the last plot in the right panel is reserved for the correlation of m_{23} against θ_y.

In Fig. 2, left panel, we present five correlations of J (against $\theta_z, \delta, \sigma, \rho$ and the LNM) and the correlation of ρ versus the LNM. As to the right panel, we include a presentation for the correlations of $\langle m \rangle_{ee}$ against θ_x, θ_z, ρ, σ, the LNM, and J.

As to Fig. 3, and in a similar way, we present correlations for θ against θ_y and δ and for $|\chi|$ versus θ_y and θ_z. The correlation of m_3 against m_{23} and m_{21} are also included. All correlations are exhibited for all three

[1]One can see this simply by noting that if all the c_is are bounded then the analyticity of the series forces them to vanish. On the other hand, one cannot have a finite number of "unbounded" expansion coefficients, otherwise we could, assuming without loss of generality two coefficients $(c_{i_1}, c_{i_2},\ i_1 < i_2)$ whose limits at $y = y_0 = \frac{\pi}{4}$ are divergent, write $c_{i_1}(y) t^{i_1} + c_{i_2}(y) t^{i_2} = g(y,t)$, where g is a well-behaved function if the infinite sum of "bounded" terms converge. It suffices then to let y, for $t_1 \neq t_2$, approach y_0 in the relation $c_{i_2}(y) = \frac{\frac{g(y,t_1)}{t_1^{i_1}} - \frac{g(y,t_2)}{t_2^{i_1}}}{t_1^{i_2-i_1} - t_2^{i_2-i_1}}$, to reach a contradiction.

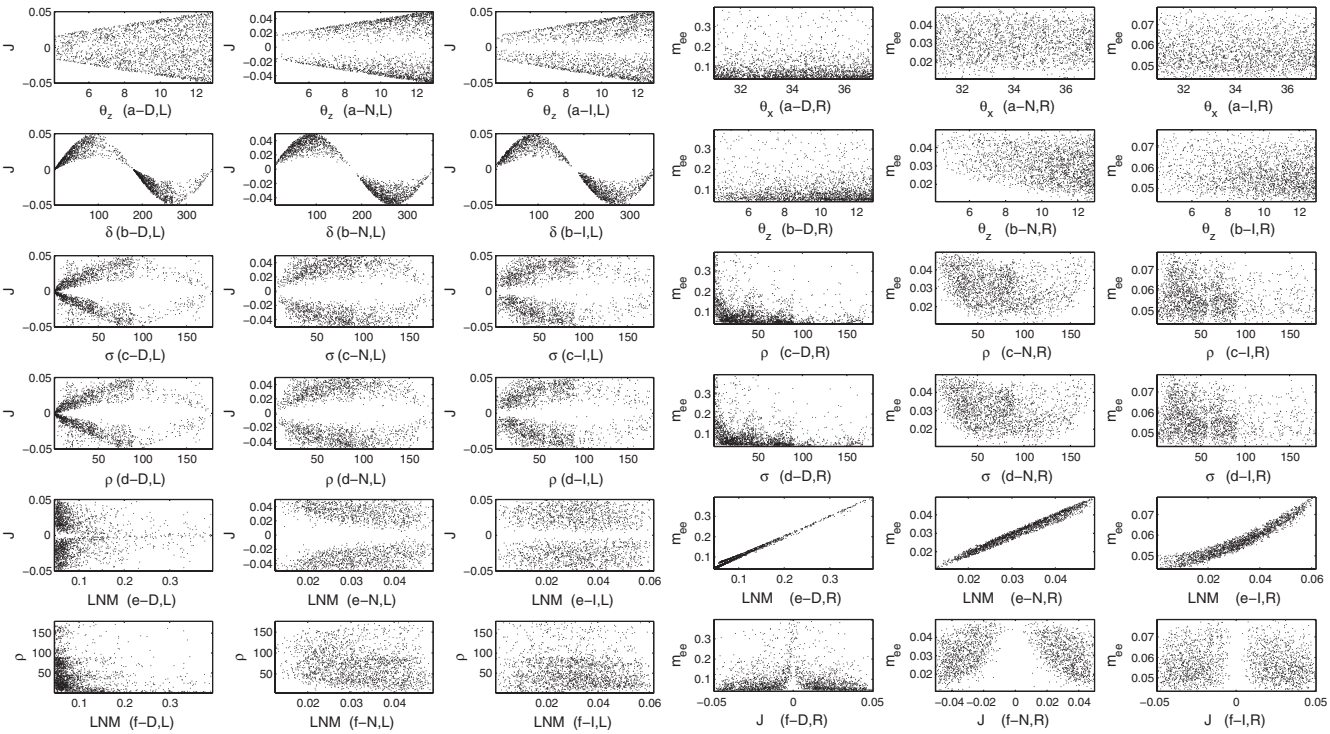

FIG. 2. Pattern having $M_{\nu 12}(1+\chi) - M_{\nu 13} = 0$, and $M_{\nu 22} - M_{\nu 33} = 0$. The left panel presents correlations of J against θ_z, δ, σ, ρ, and the LNM, while the last one depicts the correlation of the LNM against ρ. The right panel shows correlations of m_{ee} against θ_x, θ_z, ρ, σ, the LNM, and J.

types of hierarchy and for each type we have thirty-four depicted correlations.

Before dwelling on examining the correlations provided by the various figures, we can infer some restrictions concerning mixing angles and phases in each pattern just by considering the expression for R_ν as given in Eq. (52). The parameter R_ν must be positive, nonvanishing, and at the $3-\sigma$ level is restricted to be in the interval [0.0262,0.0397]. This clearly requires nonvanishing values for s_z, s_δ, s_θ, and $|\chi|$. The nonvanishing of s_z means $\theta_z \neq 0$, which is phenomenologically favorable, while the vanishing of s_δ, s_θ implies excluding 0, π, and 2π for both δ and θ. The nonvanishing of $|\chi|$ is naturally expected otherwise there would not be a deviation from exact μ–τ symmetry. The other required restriction, namely, $s_\theta s_\delta < 0$ dictates that if δ falls in the first and second quadrants, then θ falls in the third and fourth quadrants and vice versa. These conclusions remain valid if one uses the exact expression for R_ν instead of the first order expression. Explicit computations of R_ν using its exact expression tell us that θ_y cannot be exactly equal to $\frac{\pi}{4}$, otherwise R_ν would be zero, but nevertheless θ_y can possibly stay very close to $\frac{\pi}{4}$.

We see in Fig. 1 (plots a-L → c-L being examples) that all the experimentally allowed ranges of mixing angles, at 3-σ error levels, can be covered in this pattern except for normal and inverted hierarchy types where θ_y is restricted to be around 45°, by, at most, plus or minus 1.5°. This restriction on θ_y is a characteristic of the normal and inverted hierarchy type in this pattern. This characteristic behavior of θ_y can be understood by expressing the mass ratios, using Eqs. (49), (50), and (52) as

$$m_{13} = 1 - \frac{1}{2} c_x^2 R_\nu + O(s_z^2),$$
$$m_{23} = 1 + \frac{1}{2} s_x^2 R_\nu + O(s_z^2), \tag{54}$$

where the first order correction is identified consistently with R_ν expressed up to this order. All the remaining higher order corrections to the mass ratios contribute significantly and in a spiky way in the vicinity of $\theta_y = \frac{\pi}{4}$, leading to mass ratios considerably greater or smaller than unity. Therefore, to produce the various hierarchy types as marked in Eqs. (45)–(47), θ_y can take in the degenerate hierarchy type values far from $\frac{\pi}{4}$ corresponding to small higher order corrections in Eq. (54), which would keep m_{13} and m_{23} near the value one. However, in order to get normal or inverted hierarchies, the higher order corrections in Eq. (54) should contribute in a noticeably large amount, which could not happen unless θ_y stays close to $\frac{\pi}{4}$, and this is what the corresponding ranges for θ_y reported in Table III confirm. As to the Dirac CP-phase δ, the whole range is allowed except the regions around 0 and

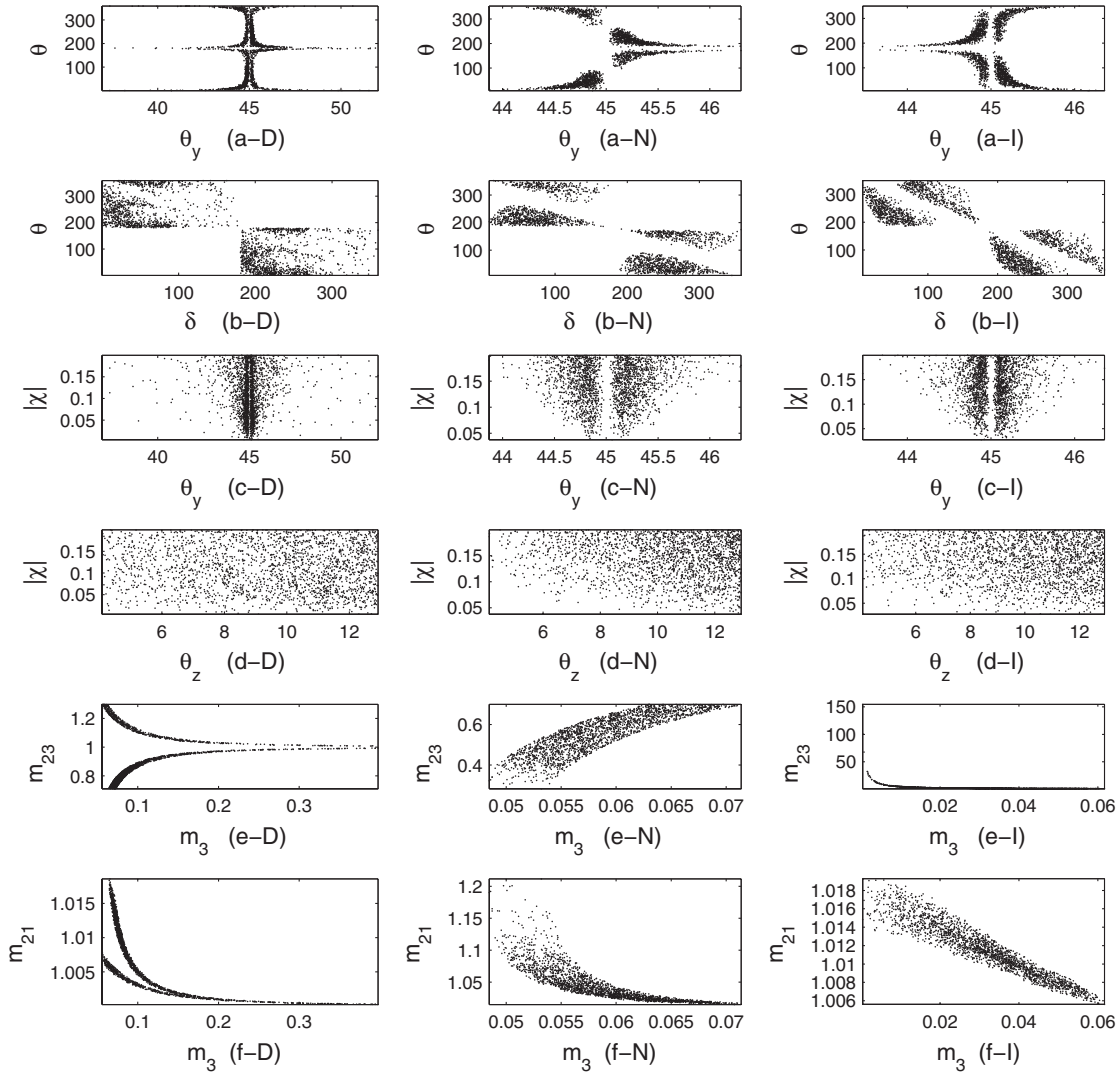

FIG. 3. Pattern having $M_{\nu 12}(1+\chi) - M_{\nu 13} = 0$, and $M_{\nu 22} - M_{\nu 33} = 0$. The first two rows present the correlations of θ against θ_y and δ, while the second two rows depict those of $|\chi|$ versus θ_y and θ_z. The last two rows show the correlations of mass ratios m_{23} and m_{21} against m_3.

π whose extensions depend on the type of hierarchy and the precision level, as evident from the same plots and the reported values in Table III. Likewise, the plots (g-L, h-L), in Fig. 1 and the values reported in Table III show that the Majorana phases (ρ, σ) are covering their ranges excluding regions around 0 and π.

The plots in Fig. 1 can reveal many obvious clear correlations. For example, the plots (a-R) show that as θ_z decreases θ_y tends to be very close to 45°. The plots (d-L, e-L) show a sort of distorted linear correlation of δ versus (ρ, σ) in all hierarchy types, which confirms the relations presented in Eq. (51) that give linear relations at zeroth order of s_z, while the found distortion can be attributed to the higher order corrections. We may also see, in plot e-R, a very clear linear correlation between the Majorona phases (ρ, σ) in all hierarchy types, which again confirms the relations presented in Eq. (51) that at the zeroth order produce the linear relation $\rho \approx \sigma$.

Figure 2 (plots a-L, b-L) shows that the correlations (J, θ_z) and (J, δ) each have a specific geometrical shape irrespective of the hierarchy type. In fact, Eq. (16) indicates that the correlation (J, δ) can be seen as a superposition of many sinusoidal graphs in δ, the "positive" amplitudes of which are determined by the acceptable mixing angles, whereas the (J, θ_z) correlation is a superposition of straight lines in $s_z \sim \theta_z$, for small θ_z, the slopes of which are positive or negative according to the sign of s_δ. The resulting shape for the (J, θ_z) correlation being trapezoidal rather than isosceles is due to the exclusion of zero and its vicinity to θ_z considering the latest oscillation data. The unfilled region in the plots originates from the disallowed region of δ around 0 and π, which would have led, if allowed, to zero J.

The left panel of Fig. 2 (plots c-L, d-L) unveils a correlation of J versus (ρ, σ) that is a direct consequence of the "linear" correlations of δ against (ρ, σ) and of the

"geometrical" correlation of (J,δ). The two correlations concerning the LNM (plots e-L, f-L) reveal that as the LNM increases the parameter space becomes more restricted. This seems to be a general tendency in all the patterns, where the LNM can reach values higher than in the normal and inverted hierarchies in the degenerate case.

To gain more insight about the correlations involving $\langle m\rangle_{ee}$ as defined in Eq. (14), we work out approximate formulas for $\langle m\rangle_{ee}$ corresponding to different hierarchy types. It is helpful in deriving these approximate formulas to realize that $\rho\approx\sigma$ and $m_1\approx m_2$ in all hierarchy types as is evident respectively from Fig. 1 (plots e-R) and Fig. 3 (plot f), and also to realize that the normal hierarchy is moderate (meaning m_3 is of the same order as m_1) while the inverted one is acute, as can be inferred from Fig. 3 (plots e-N, e-I). Thus, the resulting formulas are

$$\begin{aligned}\langle m\rangle_{ee} &\approx m_1(1-2s_z^2c_z^2s_\sigma^2)\\ &\qquad \text{for normal and degenerate cases, and}\\ \langle m\rangle_{ee} &\approx m_1(1-s_z^2) \qquad \text{for the inverted case.}\end{aligned} \tag{55}$$

The correlations of $\langle m\rangle_{ee}$ against $(\theta_x,\theta_z,\rho,\sigma)$ as depicted in the right panel of Fig. 2 (plots a-R –d-R) can be understood by exploiting the approximate expression for $\langle m\rangle_{ee}$ in conjunction with the correlations found between θ_z and (θ_x,ρ,σ). The totality of correlations of $\langle m\rangle_{ee}$ presented in the right panel of Fig. 2 indicate that the increase of $\langle m\rangle_{ee}$ would on the whole constrain the allowed parameter space. We also note a general trend of increasing $\langle m\rangle_{ee}$ with an increasing LNM in all cases of hierarchy (plots e-R). The values of $\langle m\rangle_{ee}$ cannot reach the zero limit in all types of hierarchy, as is evident from the graphs or explicitly from the corresponding covered range in Table III. Another point concerning $\langle m\rangle_{ee}$ is that its scale is triggered by the scale of m_1 ($\approx m_2$), as is evident from both the approximate formula in Eq. (55) and the corresponding covered range in Table III.

The plots in Fig. 3 (plot b) disclose a clear correlation between θ and δ that is in accordance with what was derived before in that ($s_\theta s_\delta<0$). The plots also reveal that there are disallowed regions for both θ and δ, which must definitely contain domains around 0 and π besides other possible additional areas. The disallowed regions can also be checked with the help of Tables (III)–(IV) where one additionally finds that the regions around 0 and π tend to be shrunk for the degenerate case. The plots (c) in Fig. 3 show that as θ_y deviates slightly from $\frac{\pi}{4}$ the quantity $|\chi|$ tends to increase.

For the mass spectrum, we see from Fig. 3 (plots e, f) that the normal hierarchy is mild in that the mass ratios do not reach extreme values. In contrast, the inverted hierarchy can be acute in that the mass ratio m_{23} can reach values up to $O(10^2)$. The values of m_1 and m_2 are nearly equal in all hierarchy types. We also see that if m_3 is large enough, then only the degenerate case with $m_1\sim m_2$ can be phenomenologically acceptable.

B. C2: Pattern having $M_{\nu 12}(1+\chi)+M_{\nu 13}=0$, and $M_{\nu 22}-M_{\nu 33}=0$

In this pattern, C2, the relevant expressions for As and Bs are

$$\begin{aligned}A_1 &= -c_xc_z(c_xs_ys_z+s_xc_ye^{-i\delta})(1+\chi)\\ &\quad +c_xc_z(-c_xc_ys_z+s_xs_ye^{-i\delta}),\\ A_2 &= s_xc_z(-s_xs_ys_z+c_xc_ye^{-i\delta})(1+\chi)\\ &\quad -s_xc_z(s_xc_ys_z+c_xs_ye^{-i\delta}),\\ A_3 &= s_zs_yc_z(1+\chi)+s_zc_yc_z,\\ B_1 &= (c_xs_ys_z+s_xc_ye^{-i\delta})^2-(-c_xc_ys_z+s_xs_ye^{-i\delta})^2,\\ B_2 &= (-s_xs_ys_z+c_xc_ye^{-i\delta})^2-(s_xc_ys_z+c_xs_ye^{-i\delta})^2,\\ B_3 &= s_y^2c_z^2-c_y^2c_z^2,\end{aligned} \tag{56}$$

leading to mass ratios, up to leading order in s_z, as

$$\begin{aligned}m_{13} &\approx 1-\frac{2s_\delta s_\theta|\chi|s_z}{t_xT_2},\\ m_{23} &\approx 1+\frac{2t_xs_\delta s_\theta|\chi|s_z}{T_2},\end{aligned} \tag{57}$$

where T_2 is defined as

$$T_2=|\chi|^2c_y^2+2|\chi|c_\theta c_y(c_y-s_y)+1-s_{2y}. \tag{58}$$

The Majorana phases are given by

$$\begin{aligned}\rho &\approx \delta-\frac{s_\delta s_z(s_yc_y|\chi|^2+|\chi|c_\theta(c_{2y}+s_{2y})+c_{2y})}{t_xT_2},\\ \sigma &\approx \delta+\frac{s_\delta t_xs_z(s_yc_y|\chi|^2+|\chi|c_\theta(c_{2y}+s_{2y})+c_{2y})}{T_2}.\end{aligned} \tag{59}$$

The parameters R_ν, the mass ratio square difference $m_{23}^2-m_{13}^2$, $\langle m\rangle_e$, and $\langle m\rangle_{ee}$, can be deduced to be

$$\begin{aligned}R_\nu &\approx \frac{8s_\delta s_\theta|\chi|s_z}{s_{2x}T_2},\\ m_{23}^2-m_{13}^2 &\approx \frac{8s_\delta s_\theta|\chi|s_z}{s_{2x}T_2},\\ \langle m\rangle_e &\approx m_3\left[1-\frac{4s_\theta s_\delta|\chi|s_z}{t_{2x}T_2}\right],\\ \langle m\rangle_{ee} &\approx m_3\left[1-\frac{4s_\theta s_\delta|\chi|s_z}{t_{2x}T_2}\right].\end{aligned} \tag{60}$$

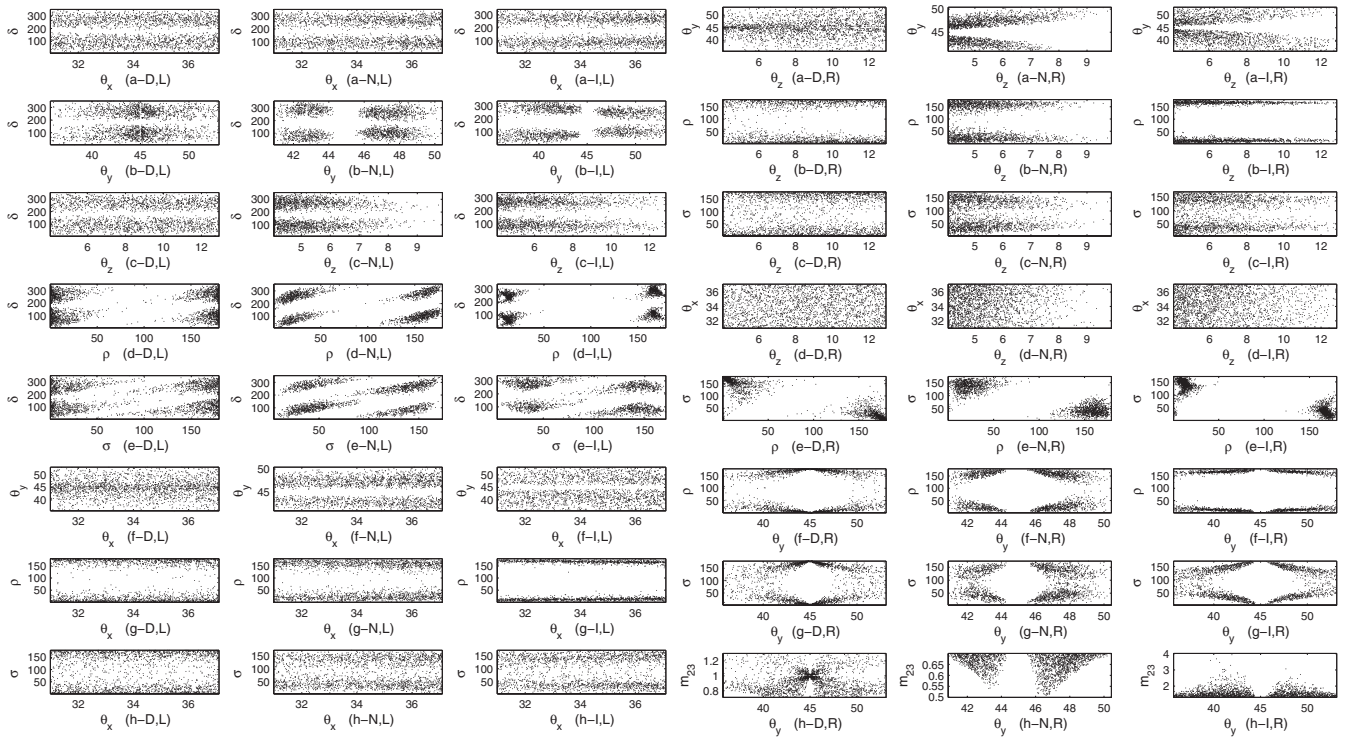

FIG. 4. Pattern having $M_{\nu 12}(1+\chi)+M_{\nu 13}=0$, and $M_{\nu 22}-M_{\nu 33}=0$. The left panel (the left three columns) presents correlations of δ against mixing angles and Majorana phases (ρ and σ) and those of θ_x against θ_y, ρ, and σ. The right panel (the right three columns) shows the correlations of θ_z against θ_y, ρ, σ, and θ_x and those of ρ against σ and θ_y, and also the correlation of θ_y versus σ and m_{23}.

One can notice that all the results concerning this pattern, C2, can be derived from those of the previous one, C1, simply by making the substitutions $s_y \to -s_y$ and $\delta \to \delta + \pi$. Unfortunately, the found relation cannot be used in practice to derive the predictions of one pattern from the other because the mapping $s_y \to -s_y$ takes θ_y from a physically admissible region to a forbidden one. However, one can also verify that the two patterns have the same properties regarding divergences for the expansion coefficients of the mass ratios.

The approximate expression for R_ν in Eq. (60) provides us with similar restrictions like those of the previous pattern C1, except that both δ and θ should now fall in the same upper or lower semicircles. Once again the derived restriction remains unchanged when using the exact expression for R_ν.

We plot the corresponding correlations in Figs. (4), (5), and (6) with the same conventions as before. In contrast to the C1 case, we see here that the mixing angle (θ_y) can cover a wider range in the normal and inverted hierarchy cases instead of being confined around $\theta_y = \frac{\pi}{4}$. In the normal hierarchy case θ_y falls in the interval $[41^\circ\text{–}50^\circ]$, while it almost covers all of the admissible range in the inverted case. In the degenerate case, however, there is no restriction on θ_y, as it was in the C1 pattern. Another contrasting feature is the range of θ_z in the normal hierarchy type, where it is now restricted to be less than 10°, and whereas it can, similarly to the C1 pattern, cover all of its allowed ranges in the inverted and degenerate cases.

We can understand the behavior of θ_y, compared to that of the previous pattern C1, by expressing the mass ratios, from Eqs. (57), (58), and (60), as

$$m_{13} = 1 - \frac{1}{2} c_x^2 R_\nu + O(s_z^2),$$
$$m_{23} = 1 + \frac{1}{2} s_x^2 R_\nu + O(s_z^2), \tag{61}$$

where the first order correction is identified consistently with R_ν expressed up to this order, and thus representing a small quantity. In contrast to the situation in the pattern C1, the remaining higher order corrections in the mass ratios can be tuned to have a significant contribution in the vicinity of any θ_y depending on the other combinations of mixing angles and phases, which would lead to mass ratios considerably greater or smaller than unity. Therefore, the various hierarchy types as marked in Eqs. (45)–(47) can be generated for almost all θ_y in its allowed range, and the values of θ_y reported in Table III confirm this. As to the Dirac *CP*-phase δ, the whole range is allowed except the regions around 0 and π, whose extensions depend on the type of hierarchy and the precision level as is evident from the corresponding plots and from the reported values in Table III.

The plots in Fig. 4 can disclose many obvious clear correlations. For example, the plots (a-R) show, in normal and inverted hierarchy cases, that as θ_z decreases θ_y tends to be spread over its admissible range while the contrary

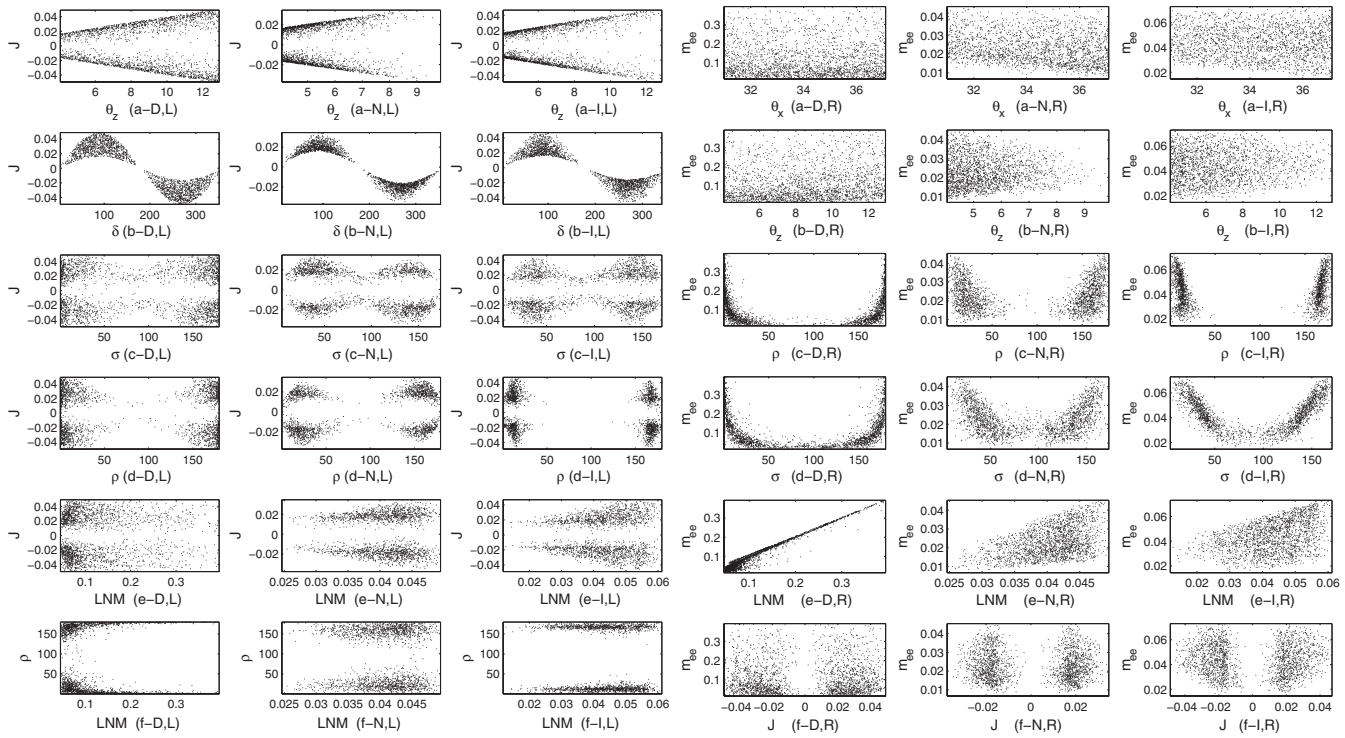

FIG. 5. Pattern having $M_{\nu 12}(1+\chi)+M_{\nu 13}=0$, and $M_{\nu 22}-M_{\nu 33}=0$. The left panel presents correlations of J against θ_z, δ, σ, ρ, and the lowest LNM, while the last one depicts the correlation of the LNM against ρ. The right panel shows correlations of m_{ee} against θ_x, θ_z, ρ, σ, the LNM, and J.

occurs when θ_z increases. The plots (d-L, e-L) do not show a simple correlation of δ versus ρ, σ in the various hierarchy types, which would have been consistent with the zeroth order linear relation given in Eq. (59). In fact, the higher order corrections bring a severe distortion that invalidates the zeroth order linear relation even at the approximate level. These higher order corrections do not work in the same manner for both ρ and σ, so they do not cancel out upon subtraction, producing an ambiguous correlation between ρ and σ, as depicted in the (plot e-R), contrasted with the simple linearity in the previous pattern C1. The absence of linear relations among the phases (δ,ρ,σ) forbids the allowed region of Majorana phases to be straightforwardly determined from that of the Dirac phase (δ), as can be figured out by looking at the corresponding allowed values in Table III.

The special "sinusoidal" and "trapezoidal" shapes of J versus δ and θ_z remain intact (Fig. 5, plots a-L, b-L), and, as before, the unfilled region in the trapezoidal shaped plots is attributed to the disallowed region for δ around 0 and π. The usual correlations of J versus ρ and σ (Fig. 5, plots c-L, d-L) emerge from those of δ versus ρ and σ. The two correlations concerning the LNM (plots e-L, f-L) indicate that as the LNM increases (say, larger than 0.1 ev) the parameter space becomes more restricted. This seems to represent an inclination in all the patterns, where the LNM can reach values higher than the other hierarchies in the degenerate case.

The correlations involving $\langle m\rangle_{ee}$ can be made more transparent by deriving an approximate formula for $\langle m\rangle_{ee}$ capturing the essential observed features for all kinds of hierarchies in this specific pattern, C2, which are, first, the equality of m_1 and m_2 as is clear in Fig. 6 (plot f); and second, the mild hierarchy in both normal and inverted cases as is evident from Fig. 6 (plots e-N, e-I). Thus, one can deduce from Eq. (14) that $\langle m\rangle_{ee}$ is approximated by

$$\langle m\rangle_{ee}\approx m_1 c_z^2\sqrt{[1-s_{2x}^2\sin^2(\rho-\sigma)]}. \tag{62}$$

Now the correlations of $\langle m\rangle_{ee}$ against $(\theta_x,\theta_z,\rho,\sigma)$, as displayed in the right panel of Fig. 5 (plots a-R–d-R) can be comprehended by invoking the approximate expression for $\langle m\rangle_{ee}$ in conjunction with the pair correlations found amidst θ_x, θ_z, ρ, and σ. The whole correlations of $\langle m\rangle_{ee}$ presented in the right panel of Fig. 5 point out that the increase of $\langle m\rangle_{ee}$ would generally constrain the allowed parameter space. We also note a general tendency of increasing $\langle m\rangle_{ee}$ with an increasing LNM in all cases of hierarchy (plots e-R). The values of $\langle m\rangle_{ee}$ cannot attain the zero limit in all types of hierarchy, as is evident from the graphs or explicitly from the corresponding covered range in Table III. Another point concerning $\langle m\rangle_{ee}$ is that its scale is triggered by the scale of m_1 ($\approx m_2$) as is evident from both the approximate formula in Eq. (62) and the corresponding covered range stated in Table III.

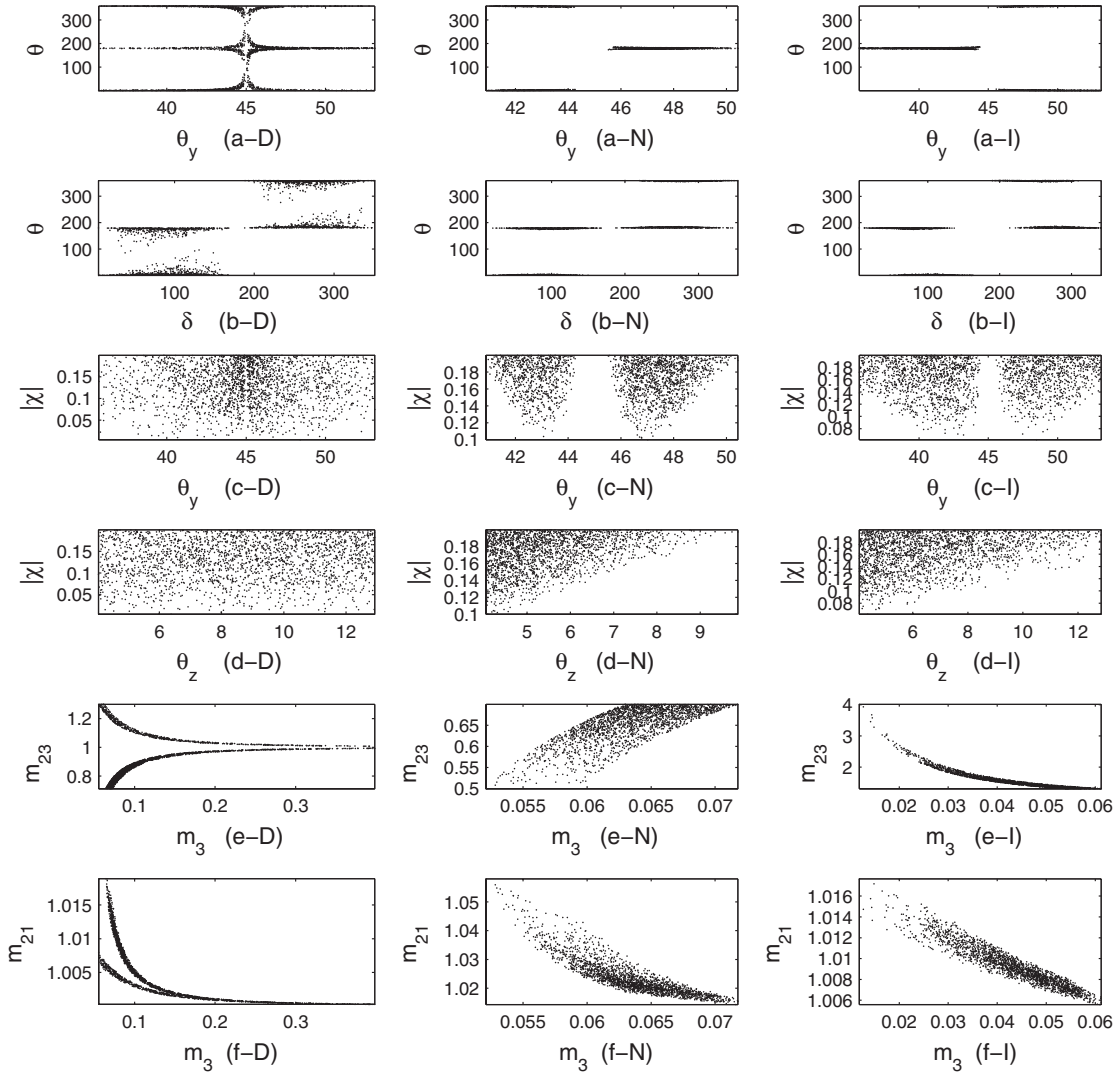

FIG. 6. Pattern having $M_{\nu 12}(1+\chi)+M_{\nu 13}=0$, and $M_{\nu 22}-M_{\nu 33}=0$. The first two rows present the correlations of θ against θ_y and δ, while the second two rows depict those of $|\chi|$ versus θ_y and θ_z. The last two rows show the correlations of mass ratios m_{23} and m_{21} against m_3.

The plots in Fig. 6 (plot b) shows both that θ and δ must lie in the same upper or lower semicircle, which confirms our inference based on the approximate formula for R_ν in Eq. (60). The plots also reveal that there are disallowed regions for both θ and δ, which definitely should contain regions around 0 and π besides other possible additional regions. The disallowed regions can also be checked with the help of Tables III–IV where one can additionally find that the forbidden regions around 0 and π tend to be shrunk for the degenerate case and that the allowed range for θ is very limited in the normal and inverted hierarchy. Figure 6 (plots c,d) shows that $|\chi|$ tends to increase in normal and inverted heirarchies as θ_y deviates from $\frac{\pi}{4}$ or as θ_z increases.

For the mass spectrum, we see from Fig. 6 (plot e) that all hierarchy types are characterized by nearly equal values of m_1 and m_2. Moreover, Fig. 6 (plot f) reveals that both normal and inverted hierarchies are of moderate type in that the mass ratios m_{23} do not reach extremely low or high values. We also see that if m_3 is large enough, then only the degenerate case with $m_1 \sim m_2$ can be compatible with the data.

C. C3: Pattern having $M_{\nu 12}-M_{\nu 13}=0$, and $M_{\nu 22}(1+\chi)-M_{\nu 33}=0$

In this pattern, the relevant expressions for As and Bs are

$$
\begin{aligned}
A_1 &= -c_x c_z(c_x s_y s_z + s_x c_y e^{-i\delta}) - c_x c_z(-c_x c_y s_z + s_x s_y e^{-i\delta}),\\
A_2 &= s_x c_z(-s_x s_y s_z + c_x c_y e^{-i\delta}) + s_x c_z(s_x c_y s_z + c_x s_y e^{-i\delta}),\\
A_3 &= s_z c_z(s_y - c_y),\\
B_1 &= (c_x s_y s_z + s_x c_y e^{-i\delta})^2(1+\chi) - (-c_x c_y s_z + s_x s_y e^{-i\delta})^2,\\
B_2 &= (-s_x s_y s_z + c_x c_y e^{-i\delta})^2(1+\chi) - (s_x c_y s_z + c_x s_y e^{-i\delta})^2,\\
B_3 &= s_y^2 c_z^2(1+\chi) - c_y^2 c_z^2,
\end{aligned}
\tag{63}
$$

leading to mass ratios, up to the leading order in s_z, as

$$m_{13} \approx \sqrt{\frac{T_3}{T_4}}\left[1 - \frac{|\chi| c_{2y}(-c_\delta s_y^2|\chi| + c_{2y}c_{\delta-\theta})s_z}{t_x(1+s_{2y})T_3}\right] + O(s_z^2),$$
$$m_{23} \approx \sqrt{\frac{T_3}{T_4}}\left[1 + \frac{|\chi| c_{2y} t_x(-c_\delta s_y^2|\chi| + c_{2y}c_{\delta-\theta})s_z}{(1+s_{2y})T_3}\right] + O(s_z^2), \tag{64}$$

where T_3 and T_4 are defined as

$$T_3 = |\chi|^2 s_y^4 - 2|\chi| c_\theta s_y^2 c_{2y} + c_{2y}^2,$$
$$T_4 = |\chi|^2 c_y^4 + 2|\chi| c_\theta c_y^2 c_{2y} + c_{2y}^2, \tag{65}$$

while the Majorana phases are defined as

$$\rho \approx \frac{1}{2}\arctan \times \left[\frac{|\chi|^2 c_y^2 s_y^2 s_{2\delta} - |\chi| c_{2y}(2c_y^2 s_{2\delta}c_\theta - s_{2\delta+\theta}) - s_{2\delta}c_{2y}^2}{|\chi|^2 c_y^2 s_y^2 c_{2\delta} - |\chi| c_{2y}(2c_y^2 c_{2\delta}c_\theta - c_{2\delta+\theta}) - c_{2\delta}c_{2y}^2}\right] + O(s_z),$$
$$\approx \delta \qquad \text{for small enough} |\chi|; |\chi| \le 0.2,$$
$$\sigma \approx \frac{1}{2}\arctan \times \left[\frac{|\chi|^2 c_y^2 s_y^2 s_{2\delta} - |\chi| c_{2y}(2c_y^2 s_{2\delta}c_\theta - s_{2\delta+\theta}) - s_{2\delta}c_{2y}^2}{|\chi|^2 c_y^2 s_y^2 c_{2\delta} - |\chi| c_{2y}(2c_y^2 c_{2\delta}c_\theta - c_{2\delta+\theta}) - c_{2\delta}c_{2y}^2}\right] + O(s_z),$$
$$\approx \delta \qquad \text{for small enough} |\chi|; |\chi| \le 0.2. \tag{66}$$

The parameters R_ν, the mass ratio square difference $m_{23}^2 - m_{13}^2$, $\langle m\rangle_e$, and $\langle m\rangle_{ee}$, can be deduced to be

$$R_\nu \approx \frac{2|\chi| c_{2y}(-c_\delta s_y^2|\chi| + c_{2y}c_{\delta-\theta})s_z}{s_x c_x (1+s_{2y})T_4} + O(s_z^2),$$
$$m_{23}^2 - m_{13}^2 \approx \frac{2|\chi| c_{2y}(-c_\delta s_y^2|\chi| + c_{2y}c_{\delta-\theta})s_z}{s_x c_x (1+s_{2y})T_4} + O(s_z^2),$$
$$\langle m\rangle_e \approx m_3\sqrt{\frac{T_3}{T_4}}\left[1 + \frac{2s_z|\chi| c_{2y}(|\chi| s_y^2 c_\delta - c_{2y}c_{\delta-\theta})}{t_{2x}(1+s_{2y})T_3}\right] + O(s_z^2),$$
$$\langle m\rangle_{ee} \approx m_3\sqrt{\frac{T_3}{T_4}}\left[1 + \frac{2s_z|\chi| c_{2y}(|\chi| s_y^2 c_\delta - c_{2y}c_{\delta-\theta})}{t_{2x}(1+s_{2y})T_3}\right] + O(s_z^2). \tag{67}$$

It is noteworthy that the expansions in terms of s_z for this pattern are well behaved in the sense that the expansion coefficients appearing in the mass ratio expressions are not divergent for certain values of the mixing angles as is the case in the C1 and C2 patterns. Therefore, the expansion can be reliably used as a perturbative expansion in which higher order terms have a negligible contribution compared to the lower ones. In this pattern, it remains forbidden for θ_z or the difference $(\theta_y - \frac{\pi}{4})$ to vanish; otherwise, as exact computations show, we would have degeneracy for m_1 and m_2 leading to vanishing R_ν. In contrast, the phases δ (Dirac phase) and θ can attain the values zero or π without implying vanishing R_ν. These findings can be easily deduced using the approximate formula for R_ν as given in Eq. (67). The complete degeneracy $(m_1 = m_2 = m_3)$ is achieved when $\theta_y = \frac{\pi}{4}$ and $\delta = \frac{\pi}{2}$, which can only be checked using the exact complicated formulas for m_{13} and m_{23}. At this particular value, $(\theta_y = \frac{\pi}{4},\ \delta = \frac{\pi}{2})$, the zeroth order expansion coefficient, of say $m_{13}\sqrt{T4/T3}$, assumes the value of one, while the other remaining coefficients are checked to be vanishing. The positivity of R_ν and the constraint to lie within the interval [0.0262,0.0397] (at the $3-\sigma$ level) imposes a complicated relation between δ and θ rather than the simple constraint of belonging to alternate (identical) semicircles in the cases C1 (C2).

The phenomenology of this pattern has many features in common with that of the pattern C1 in terms of correlations and allowed values for the parameters, as can checked from the corresponding Figs. 7–9 versus 1–3 and Tables III–IV. Thus, we shall not repeat the same discussions and descriptions. Rather, we mention a few dissimilarities: first, the mixing angle θ_y is allowed to cover all of its admissible range even in the cases of inverted and normal hierarchies; second, the correlation between δ and θ is not as simple as that of belonging to opposite semicircles in the pattern C1, where the R_ν's expression allows us to interpret it.

D. C4: Pattern having $M_{\nu 12} + M_{\nu 13} = 0$, and $M_{\nu 22}(1+\chi) - M_{\nu 33} = 0$

In this pattern, the relevant expressions for As and Bs are

$$A_1 = -c_x c_z(c_x s_y s_z + s_x c_y e^{-i\delta}) + c_x c_z(-c_x c_y s_z + s_x s_y e^{-i\delta}),$$
$$A_2 = s_x c_z(-s_x s_y s_z + c_x c_y e^{-i\delta}) - s_x c_z(s_x c_y s_z + c_x s_y e^{-i\delta}),$$
$$A_3 = s_z c_z(s_y + c_y),$$
$$B_1 = (c_x s_y s_z + s_x c_y e^{-i\delta})^2(1+\chi) - (-c_x c_y s_z + s_x s_y e^{-i\delta})^2,$$
$$B_2 = (-s_x s_y s_z + c_x c_y e^{-i\delta})^2(1+\chi) - (s_x c_y s_z + c_x s_y e^{-i\delta})^2,$$
$$B_3 = s_y^2 c_z^2(1+\chi) - c_y^2 c_z^2, \tag{68}$$

leading to mass ratios, up to the leading order in s_z, as

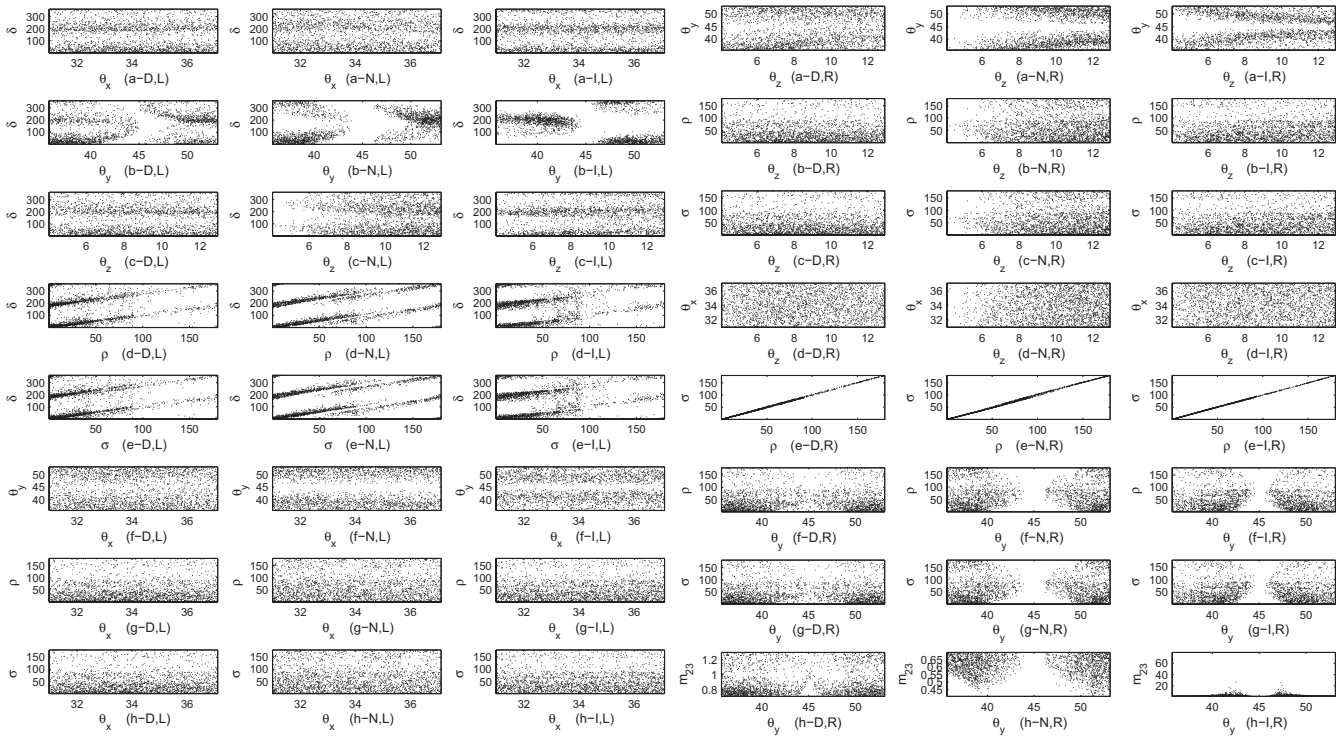

FIG. 7. Pattern having $M_{\nu 12} - M_{\nu 13} = 0$, and $M_{\nu 22}(1+\chi) - M_{\nu 33} = 0$. The left panel (the left three columns) presents correlations of δ against mixing angles and Majorana phases (ρ and σ) and those of θ_x against θ_y, ρ, and σ. The right panel (the right three columns) shows the correlations of θ_z against θ_y, ρ, σ, and θ_x and those of ρ against σ and θ_y, and also the correlation of θ_y versus σ and m_{23}.

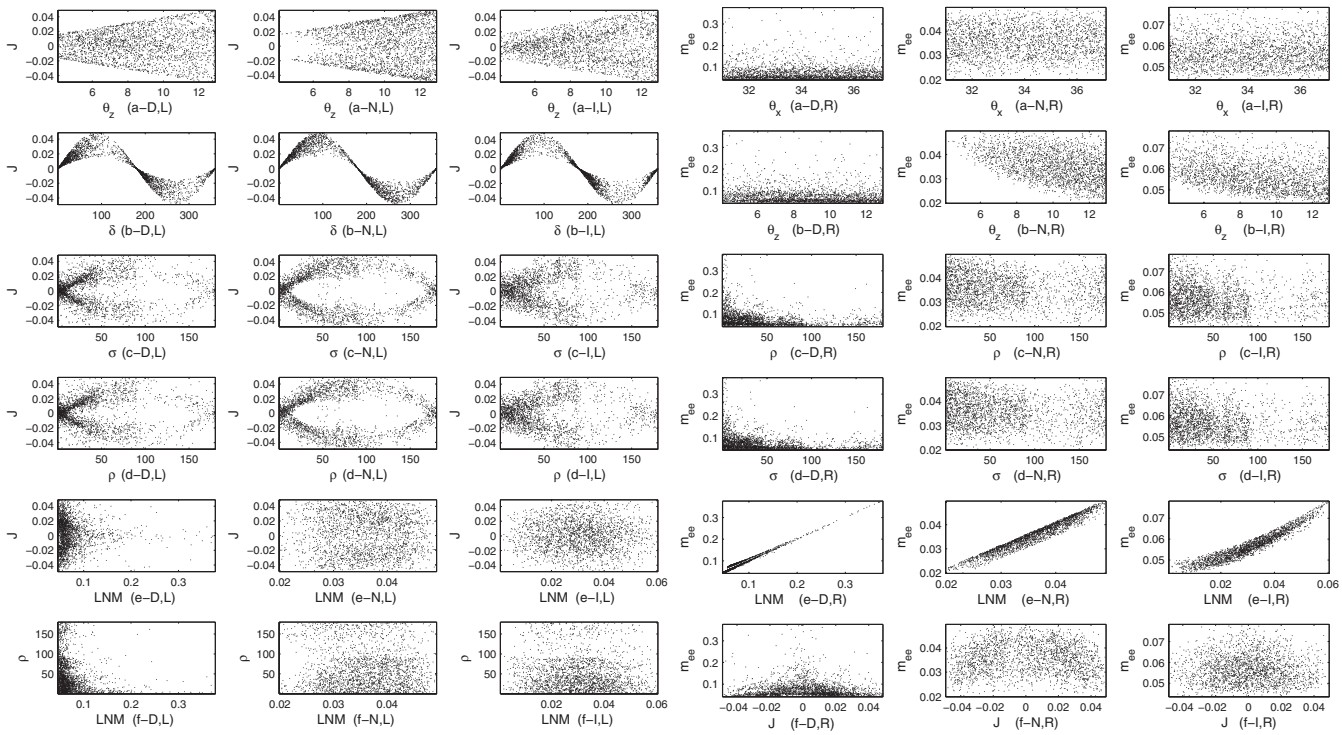

FIG. 8. Pattern having $M_{\nu 12} - M_{\nu 13} = 0$, and $M_{\nu 22}(1+\chi) - M_{\nu 33} = 0$. The left panel presents correlations of J against θ_z, δ, σ, ρ, and the LNM, while the last one depicts the correlation of the LNM against ρ. The right panel shows correlations of m_{ee} against θ_x, θ_z, ρ, σ, the LNM, and J.

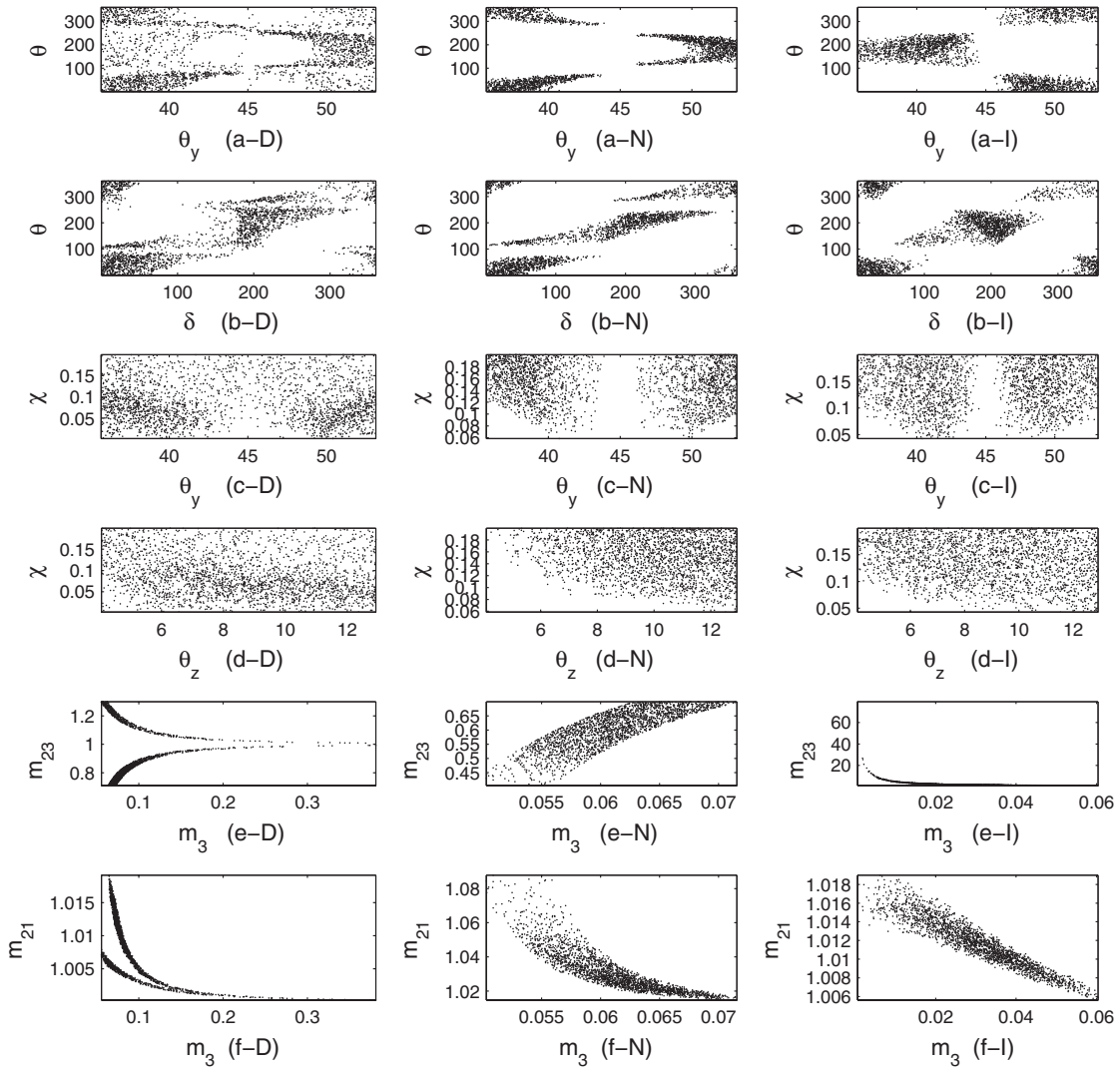

FIG. 9. Pattern having $M_{\nu 12} - M_{\nu 13} = 0$, and $M_{\nu 22}(1+\chi) - M_{\nu 33} = 0$. The first two rows present the correlations of θ against θ_y and δ, while the second two rows depict those of $|\chi|$ versus θ_y and θ_z. The last two rows show the correlations of the mass ratios m_{23} and m_{21} against m_3.

$$m_{13} \approx \sqrt{\frac{T_3}{T_4}}\left[1 + \frac{|\chi| c_{2y}(-c_\delta s_y^2 |\chi| + c_{2y} c_{\delta-\theta}) s_z}{t_x (1 - s_{2y}) T_3}\right] + O(s_z^2),$$
$$m_{23} \approx \sqrt{\frac{T_3}{T_4}}\left[1 - \frac{|\chi| c_{2y} t_x(-c_\delta s_y^2 |\chi| + c_{2y} c_{\delta-\theta}) s_z}{(1 - s_{2y}) T_3}\right] + O(s_z^2), \tag{69}$$

while the Majorana phases are as

$$\rho \approx \frac{1}{2}\arctan\left[\frac{|\chi|^2 c_y^2 s_y^2 s_{2\delta} - |\chi| c_{2y}(2 c_y^2 s_{2\delta} c_\theta - s_{2\delta+\theta}) - s_{2\delta} c_{2y}^2}{|\chi|^2 c_y^2 s_y^2 c_{2\delta} - |\chi| c_{2y}(2 c_y^2 c_{2\delta} c_\theta - c_{2\delta+\theta}) - c_{2\delta} c_{2y}^2}\right] + O(s_z),$$
$$\sigma \approx \frac{1}{2}\arctan\left[\frac{|\chi|^2 c_y^2 s_y^2 s_{2\delta} - |\chi| c_{2y}(2 c_y^2 s_{2\delta} c_\theta - s_{2\delta+\theta}) - s_{2\delta} c_{2y}^2}{|\chi|^2 c_y^2 s_y^2 c_{2\delta} - |\chi| c_{2y}(2 c_y^2 c_{2\delta} c_\theta - c_{2\delta+\theta}) - c_{2\delta} c_{2y}^2}\right] + O(s_z). \tag{70}$$

The parameters R_ν, the mass ratio square difference $m_{23}^2 - m_{13}^2$, $\langle m \rangle_e$, and $\langle m \rangle_{ee}$, can be deduced to be

$$
\begin{aligned}
R_\nu &\approx \frac{2|\chi|c_{2y}(+c_\delta s_y^2|\chi| - c_{2y}c_{\delta-\theta})s_z}{s_x c_x(1-s_{2y})T_4} + O(s_z^2),\\
m_{23}^2 - m_{13}^2 &\approx \frac{2|\chi|c_{2y}(+c_\delta s_y^2|\chi| - c_{2y}c_{\delta-\theta})s_z}{s_x c_x(1-s_{2y})T_4} + O(s_z^2),\\
\langle m\rangle_e &\approx m_3\sqrt{\frac{T_3}{T_4}}\left[1 - \frac{2s_z|\chi|c_{2y}(|\chi|s_y^2 c_\delta - c_{2y}c_{\delta-\theta})}{t_{2x}(1-s_{2y})T_3}\right] + O(s_z^2),\\
\langle m\rangle_{ee} &\approx m_3\sqrt{\frac{T_3}{T_4}}\left[1 - \frac{2s_z|\chi|c_{2y}(|\chi|s_y^2 c_\delta - c_{2y}c_{\delta-\theta})}{t_{2x}(1-s_{2y})T_3}\right] + O(s_z^2).
\end{aligned}
\tag{71}
$$

Once again, and as it was for the two patterns C1 and C2, one can find the same interrelations between C3 and C4 where the results (formulas) of C4 can be derived from those of C3, by simply making the substitutions $s_y \to -s_y$ and $\delta \to \delta + \pi$. Another time, the found relations cannot be used in a useful way to derive the predictions of one pattern from the other because the mapping $s_y \to -s_y$ does not keep the physically admissible region of θ_y invariant. Furthermore, we are ill fated in that the properties regarding the boundedness of the expansion coefficients of the mass ratios are mapped so that the bounded coefficient at $(\theta_y = \frac{\pi}{4}, \delta = \frac{\pi}{2})$ in the pattern C3 may become divergent in the case of C4. This becomes clear by looking at the expressions in Eq. (69), where the zeroth order expansion coefficient, for say $m_{13}\sqrt{T_4/T_3}$, assumes the value one, and the first order coefficient is convergent at $(\theta_y = \frac{\pi}{4}, \delta = \frac{\pi}{2})$, whereas all higher order expansion coefficients are divergent at this point while they were vanishing in the C3 pattern. This finding is consistent with the infinite number of divergent terms summing up to a smooth function as was discussed in Sec. 7 A. The divergence for R_ν expansion is starting from the second order coefficient in harmony with the corresponding behavior in the patterns C1 and C2. Using the exact expression of R_ν corresponding to this pattern shows that the mixing angle θ_y is allowed to be exactly $\frac{\pi}{4}$ without forcing R_ν to vanish. The phases δ and θ can also assume any arbitrary values, but we should note that the point $(\theta_y = \frac{\pi}{4}, \delta = \frac{\pi}{2})$ causes the exact form of R_ν to be null. It is obvious that vanishing θ_z leads also to vanishing R_ν, but this choice is already excluded by the data. As was the case in the C3 pattern, the correlation between δ and θ that emerges from the positivity of R_ν and its allowed range cannot, due to the complicated expression of R_ν that involves complicated dependence on phases even at the approximate level, be described in a simple manner. We stress again that the expansion should be dealt with and interpreted with caution in case of divergent coefficients and cannot be reliably used as a perturbative expansion. Thus, to avoid these kinds of problems, our numerical results are based on exact expressions that do not suffer from divergences.

We checked when we spanned the parameter space that the normal hierarchy could accommodate the data only at the $3-\sigma$ error level, whereas the inverted hierarchy could do it at the $2-3\sigma$ error levels, and the degenerate hierarchy could survive at all error levels. Figs. (10), (11), and (12) show the corresponding correlation plots, with the same conventions as in the previous patterns. The appearance of the normal hierarchy only at the $3-\sigma$ error level makes it so special, and it turns out to be quite restrictive in the sense that the mixing angle θ_y is severely bounded to be around two possible values, namely, 36° or 52°, whereas θ_z has only one narrow band close to 4°, while the Dirac phase δ covers almost all its range excluding the region $[158° - 188.4°]$. Moreover, in this normal hierarchy case the parameter χ, parametrizing the deviation from exact μ–τ symmetry, cannot assume an arbitrary value in its prescribed range: $|\chi|$ must be in the range [0.16–0.2], whereas the phase θ can cover all its allowable range excluding the region $]19.47° - 139.9°[\bigcup]217.4° - 340.8°[$.

Once again, there is a close resemblance between the pattern C4 and C2 in terms of correlations and allowed values for the parameters, as can be checked respectively from the corresponding Figs. 10–12 versus 4–6 and Tables III–IV. Therefore, it is not necessary to repeat the same discussions and descriptions but rather to focus on the few dissimilarities: First, the mixing angle θ_y is allowed to cover all of its admissible range in the inverted hierarchy type, and in particular the value $\frac{\pi}{4}$ which is excluded with its small neighborhood in the pattern C2; second, the Dirac phase δ is allowed to cover all of its ranges in the inverted and degenerate hierarchy types without any exclusion, as was the case in the pattern C2 concerning the values (0, and π) together with their neighborhoods; third, the mixing angle θ_z tends to have a far more restrictive range in the case of the pattern C4 compared to that of C2; fourth, the normal hierarchy case for the pattern C4, as explained above, represents an exceptional situation,

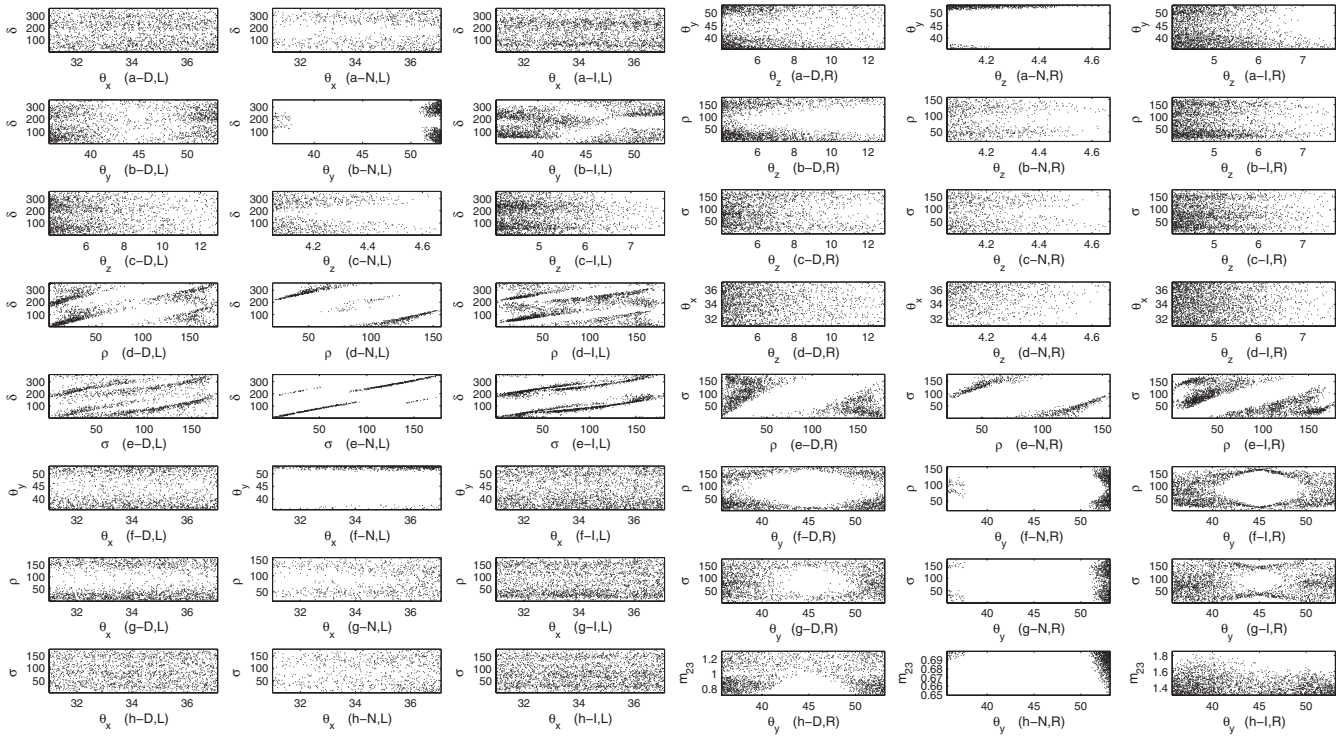

FIG. 10. Pattern having $M_{\nu 12} + M_{\nu 13} = 0$, and $M_{\nu 22}(1+\chi) - M_{\nu 33} = 0$. The left panel (the left three columns) presents correlations of δ against mixing angles and Majorana phases (ρ and σ) and those of θ_x against θ_y, ρ, and σ. The right panel (the right three columns) shows the correlations of θ_z against θ_y, ρ, σ, and θ_x and those of ρ against σ and θ_y, and also the correlation of θ_y versus σ and m_{23}.

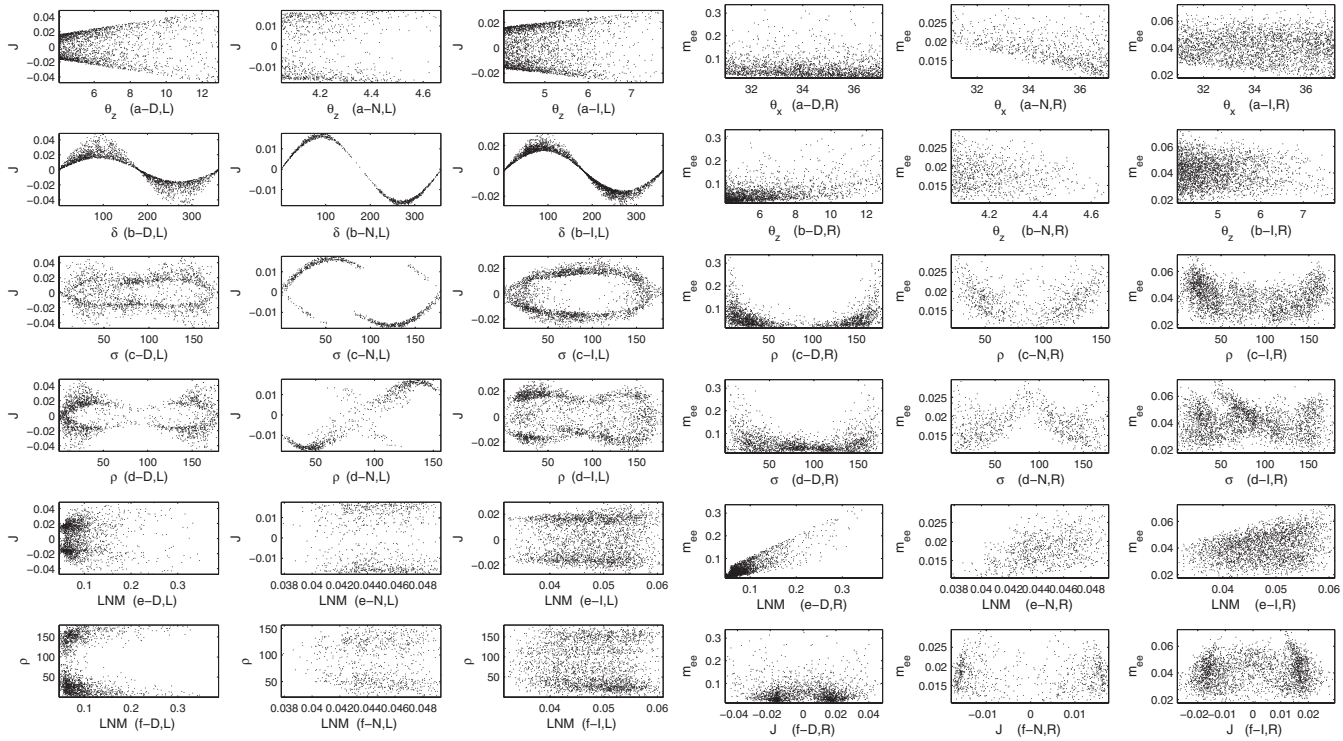

FIG. 11. Pattern having $M_{\nu 12} + M_{\nu 13} = 0$, and $M_{\nu 22}(1+\chi) - M_{\nu 33} = 0$. The left panel presents correlations of J against θ_z, δ, σ, ρ, and the LNM, while the last one depicts the correlation of the LNM against ρ. The right panel shows correlations of m_{ee} against θ_x, θ_z, ρ, σ, the LNM and J.

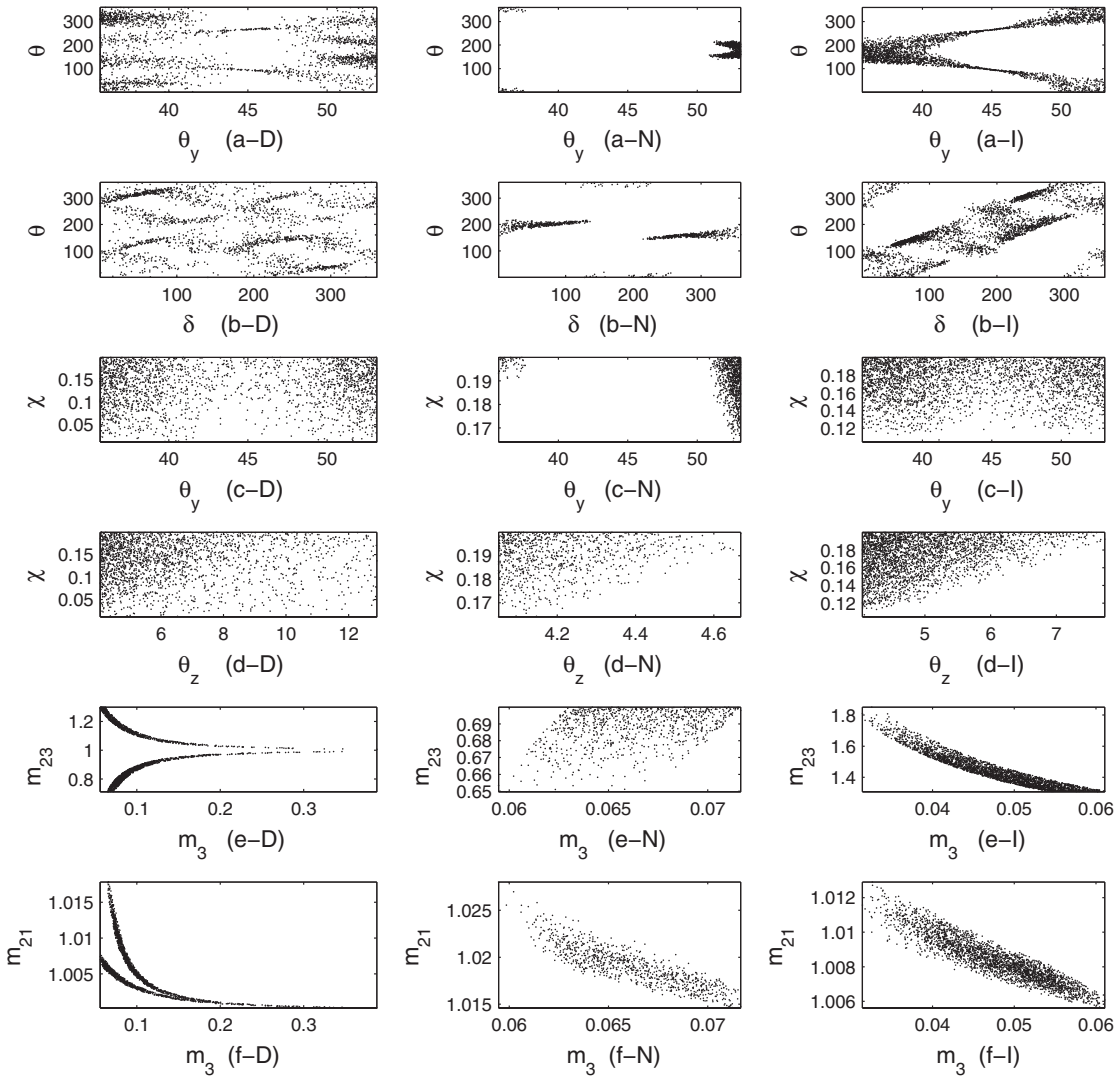

FIG. 12. Pattern having $M_{\nu 12} + M_{\nu 13} = 0$, and $M_{\nu 22}(1+\chi) - M_{\nu 33} = 0$. The first two rows present the correlations of θ against θ_y and δ, while the second two rows depict those of $|\chi|$ versus θ_y and θ_z. The last two rows show the correlations of the mass ratios m_{23} and m_{21} against m_3.

which was not the case in the pattern C2. The figures depicting the correlations for the two patterns C2 and C4 look, more or less, similar provided the loose restrictions on θ_y and δ associated with the pattern C4 are taken into consideration.

VIII. SINGULAR PATTERNS VIOLATING EXACT μ–τ SYMMETRY

As was the case in the exact symmetry, the violation of exact μ–τ symmetry does not allow for the singular neutrino mass matrix. The same analysis and arguments against the viability of the singular patterns having exact μ–τ symmetry in Sec. V can be carried out here to show the inviability of the various singular deformed patterns. The numerical study based on scanning all acceptable ranges for the mixing angles and the Dirac phase δ assures the absence of any solution satisfying the mass ratio constraints as expressed in Eq. (30) and Eq. (35). All the relevant formulas for mass ratios are collected in Table V in order to ease judging the inviability of patterns. The T_3 and T_4 present in the formulas are the ones defined in Eq. (65), while T_5 is introduced as

$$T_5 = |\chi|^2 c_y^2 c_\delta + |\chi|[c_\delta c_\theta(4c_y^2 - 1) + s_\theta s_\delta] + 2c_\delta c_{2y}. \tag{72}$$

IX. EXACT μ–τ SYMMETRY AND REALIZATIONS OF THE PERTURBED TEXTURES

We study now in detail how the perturbed textures can arise assuming an exact μ–τ symmetry at the Lagrangian level but at the expense of introducing new matter fields

TABLE V. The approximate mass ratio formulas for the singular light neutrino mass violating exact μ–τ symmetry. The formulas are calculated in terms of A's and B's coefficients.

Pattern	$m_1 = 0$ $\frac{m_2}{m_3}$	
C1	$\lvert\frac{A_3}{A_2}\rvert \approx \sqrt{\frac{\lvert\chi\rvert^2 s_y^2+2\lvert\chi\rvert c_\theta s_y(s_y-c_y)+1-s_{2y}}{\lvert\chi\rvert^2 c_y^2+2\lvert\chi\rvert c_\theta s_y(s_y+c_y)+1+s_{2y}}}\frac{s_z}{s_x c_x}+O(s_z^2)$	$\lvert\frac{B_3}{B_2}\rvert \approx \frac{1}{c_x^2}(1+2t_x t_{2y} c_\delta s_z)+O(s_z^2)$
C2	$\lvert\frac{A_3}{A_2}\rvert \approx \sqrt{\frac{\lvert\chi\rvert^2 s_y^2+2\lvert\chi\rvert c_\theta s_y(s_y+c_y)+1+s_{2y}}{\lvert\chi\rvert^2 c_y^2+2\lvert\chi\rvert c_\theta s_y(c_y-s_y)+1-s_{2y}}}\frac{s_z}{s_x c_x}+O(s_z^2)$	$\lvert\frac{B_3}{B_2}\rvert \approx \frac{1}{c_x^2}(1+2t_x t_{2y} c_\delta s_z)+O(s_z^2)$
C3	$\lvert\frac{A_3}{A_2}\rvert \approx \sqrt{\frac{1-s_{2y}}{1+s_{2y}}}\frac{s_z}{s_x c_x}+O(s_z^2)$	$\lvert\frac{B_3}{B_2}\rvert \approx \frac{1}{c_x^2}\sqrt{\frac{T_3}{T_4}}(1+\frac{t_x s_{2y} T_5 s_z}{T_4})+O(s_z^2)$
C4	$\lvert\frac{A_3}{A_2}\rvert \approx \sqrt{\frac{1+s_{2y}}{1-s_{2y}}}\frac{s_z}{s_x c_x}+O(s_z^2)$	$\lvert\frac{B_3}{B_2}\rvert \approx \frac{1}{c_x^2}\sqrt{\frac{T_3}{T_4}}(1+\frac{t_x s_{2y} T_5 s_z}{T_4})+O(s_z^2)$
Pattern	$m_3 = 0$ $\frac{m_2}{m_1}$	
C1	$\lvert\frac{A_1}{A_2}\rvert \approx 1+\frac{\lvert\chi\rvert^2 s_y c_y c_\delta+\lvert\chi\rvert[c_\delta c_\theta(s_{2y}-c_{2y})-s_\theta s_\delta]-c_\delta c_{2y}}{\lvert\chi\rvert^2 c_y^2+2\lvert\chi\rvert c_\theta c_y(s_y+c_y)+1+s_{2y}}\frac{s_z}{s_x c_x}+O(s_z^2)$	$\lvert\frac{B_1}{B_2}\rvert \approx t_x^2(1+\frac{2t_{2y}c_\delta s_z}{s_x c_x})+O(s_z^2)$
C2	$\lvert\frac{A_1}{A_2}\rvert \approx 1+\frac{\lvert\chi\rvert^2 s_y c_y c_\delta+\lvert\chi\rvert[c_\delta c_\theta(s_{2y}+c_{2y})+s_\theta s_\delta]+c_\delta c_{2y}}{\lvert\chi\rvert^2 c_y^2+2\lvert\chi\rvert c_\theta c_y(c_y-s_y)+1-s_{2y}}\frac{s_z}{s_x c_x}+O(s_z^2)$	$\lvert\frac{B_1}{B_2}\rvert \approx t_x^2(1+\frac{2t_{2y}c_\delta s_z}{s_x c_x})+O(s_z^2)$
C3	$\lvert\frac{A_1}{A_2}\rvert \approx 1-\frac{(1-s_{2y})c_\delta s_z}{c_{2y}s_x c_x}+O(s_z^2)$	$\lvert\frac{B_1}{B_2}\rvert \approx t_x^2(1+\frac{T_5 s_{2y} s_z}{T_4 s_x c_x})+O(s_z^2)$
C4	$\lvert\frac{A_1}{A_2}\rvert \approx 1+\frac{(1+s_{2y})c_\delta s_z}{c_{2y}s_x c_x}+O(s_z^2)$	$\lvert\frac{B_1}{B_2}\rvert \approx t_x^2(1+\frac{T_5 s_{2y} s_z}{T_4 s_x c_x})+O(s_z^2)$

and symmetries. To fix the ideas, let's take the $C1$ pattern put in the form

$$M_\nu = \begin{pmatrix} A & B & B(1+\chi) \\ B & C & D \\ B(1+\chi) & D & C \end{pmatrix}. \tag{73}$$

The exact μ–τ symmetry (the S symmetry) corresponding to this pattern is given by the matrix

$$S = \begin{pmatrix} 1 & 0 & 0 \\ 0 & 0 & 1 \\ 0 & 1 & 0 \end{pmatrix} \tag{74}$$

in that we have $S^2 = 1$ and

$$\{(M = M^{\mathrm{T}}) \wedge [S^{\mathrm{T}} \cdot M \cdot S = M]\} \Leftrightarrow \left[\exists A, B, C, D\colon\ M = \begin{pmatrix} A & B & B \\ B & C & D \\ B & D & C \end{pmatrix}\right]. \tag{75}$$

We shall also need the following relations:

$$\{(M = M^{\mathrm{T}}) \wedge [S^{\mathrm{T}} \cdot M \cdot S = -M]\} \Leftrightarrow \left[\exists B, C\colon\ M = \begin{pmatrix} 0 & B & -B \\ B & C & 0 \\ -B & 0 & -C \end{pmatrix}\right], \tag{76}$$

$$[S^{\mathrm{T}} \cdot M \cdot S = M] \Leftrightarrow \left[\exists A, B, C, D\colon\ M = \begin{pmatrix} A & B & B \\ E & C & D \\ E & D & C \end{pmatrix}\right], \tag{77}$$

$$[S^{\mathrm{T}} \cdot M \cdot S = -M] \Leftrightarrow \left[\exists B, C, D\colon\ M = \begin{pmatrix} 0 & B & -B \\ E & C & D \\ -E & -D & -C \end{pmatrix}\right], \tag{78}$$

$$[S \cdot M = M] \Leftrightarrow \left[\exists A, B, C, D, E, F\colon\ M = \begin{pmatrix} A & B & C \\ D & E & F \\ D & E & F \end{pmatrix}\right]. \tag{79}$$

We shall achieve the texture of Eq. (73) using both types II and I of the seesaw mechanism.

A. Type II seesaw

In the type II seesaw [40] mechanism, we now show how one can reach the desired form by assuming a flavor symmetry of the form $S \times Z_2$ and by having three Higgs triplets for the neutrino mass matrix and three Higgs doublets for the charged lepton mass matrix.

1. Matter content and symmetries

First, we extend the SM by introducing three $SU(2)_L$ scalar triplets H_a, $(a = 1, 2, 3)$,

$$H_a \equiv [H_a^{++}, H_a^{+}, H_a^{0}]. \tag{80}$$

In addition to the S symmetry, we introduce another Z_2 symmetry, and we assume the following transformations:

$$L \xrightarrow{S} SL, \qquad L \xrightarrow{Z_2} \mathrm{diag}(1,-1,-1)L \tag{81}$$

$$H \xrightarrow{S} \mathrm{diag}(1,1,-1)H, \qquad H \xrightarrow{Z_2} \mathrm{diag}(1,-1,-1)H \tag{82}$$

where the $H^{\mathrm{T}} = (H_1, H_2, H_3)$, $L^{\mathrm{T}} = (L_1, L_2, L_3)$ with L_is $(i = 1, 2, 3)$ being the components of the i^{th}-family LH lepton doublets (we shall adopt this notation of "vectors" in flavor space even for other fields, like l^c, ν_R, and $\phi, \ldots$). Note that the assignments of L_2, L_3 should be the same under Z_2 as the S symmetry interchanges them, otherwise the factor subgroups S and Z_2 do not commute. For this reason, the S-charges of H_2, H_3 are allowed to be different because Z_2 acts on H diagonally. There will also be the RH charged lepton singlets and the Higgs fields responsible for the charged lepton mass matrix.

2. Neutrino mass matrix

The Yukawa interaction relevant for neutrino mass has the form

$$\mathcal{L}_{H,L} = \sum_{i,j=1}^{3}\sum_{a=1}^{3} G_{ij}^{a}[H_a^0 \nu_{Li}^T \mathcal{C}\nu_{Lj} + H_a^{+}(\nu_{Li}^T \mathcal{C} l_{Lj} + l_{Lj}^T \mathcal{C}\nu_{Li}) + H_a^{++} l_{Li}^T \mathcal{C} l_{Lj}], \tag{83}$$

where G_{ij}^a are Yaukawa coupling constants, the indices i, j are flavor ones, and $\mathcal{C}$ is the charge conjugation matrix.

The field H_a^0 can get a small vacuum expectation value (vev), $\langle H_a^0 \rangle_0 = v_a$ leading to a Majorana neutrino mass matrix,

$$M_{\nu ij} = \sum_{a=1}^{3} G_{ij}^{a} \langle H_a^0 \rangle_0. \tag{84}$$

The smallness of the vev $\langle H_a^0 \rangle_0$ is due to the largeness of the triplet scalar mass scale [40].

The bilinear of $\nu_{Li}\nu_{Lj}$ relevant for the Majorana mass matrix transforms, via Eq. (81), under Z_2 as

$$\nu_{Li}\nu_{Lj} \overset{Z_2}{\sim} B = \begin{pmatrix} 1 & -1 & -1 \\ -1 & 1 & 1 \\ -1 & 1 & 1 \end{pmatrix},$$

$$\text{meaning } \nu_{Li}\nu_{Lj} \xrightarrow{Z_2} Z_2(\nu_{Li}\nu_{Lj}) = B_{ij}\nu_{Li}\nu_{Lj} \,(\text{no sum}). \tag{85}$$

Thus, we have

$$\left.\begin{array}{c} S^{\mathrm{T}} G^1 S = G^1, G^{1\mathrm{T}} = G^1 \\ G_{ij}^1 Z_2(H_1) Z_2(\nu_{Li}\nu_{Lj}) = G_{ij}^1 H_1 \nu_{Li}\nu_{Lj} (\text{no sum}) \end{array}\right\} \overset{\text{Eqs.75,82,85}}{\Rightarrow} G^1 = \begin{pmatrix} A^1 & 0 & 0 \\ 0 & C^1 & D^1 \\ 0 & D^1 & C^1 \end{pmatrix} \tag{86}$$

$$\left.\begin{array}{c} S^{\mathrm{T}} G^2 S = G^2, G^{2\mathrm{T}} = G^2 \\ G_{ij}^2 Z_2(H_2) Z_2(\nu_{Li}\nu_{Lj}) = G_{ij}^2 H_2 \nu_{Li}\nu_{Lj} (\text{no sum}) \end{array}\right\} \overset{\text{Eqs.75,82,85}}{\Rightarrow} G^2 = \begin{pmatrix} 0 & B^2 & B^2 \\ B^2 & 0 & 0 \\ B^2 & 0 & 0 \end{pmatrix}. \tag{87}$$

The two Higgs fields H_1, H_2 generate the unperturbed texture, whereas the perturbation is generated by the field H_3:

$$\left.\begin{array}{c} S^{\mathrm{T}} G^3 S = -G^3, G^{3\mathrm{T}} = G^3 \\ G_{ij}^3 Z_2(H_3) Z_2(\nu_{Li}\nu_{Lj}) = G_{ij}^3 H_3 \nu_{Li}\nu_{Lj} (\text{no sum}) \end{array}\right\} \overset{\text{Eqs.76,82,85}}{\Rightarrow} G^3 = \begin{pmatrix} 0 & B^3 & -B^3 \\ B^3 & 0 & 0 \\ -B^3 & 0 & 0 \end{pmatrix}. \tag{88}$$

The mass matrix we get is of the form

$$M_\nu = \begin{pmatrix} v_1 A^1 & v_2 B^2 + v_3 B^3 & v_2 B^2 - v_3 B^3 \\ v_2 B^2 + v_3 B^3 & v_1 C^1 & v_1 D^1 \\ v_2 B^2 - v_3 B^3 & v_1 D^1 & v_1 C^1 \end{pmatrix}. \tag{89}$$

Thus, if the Yukawa couplings are all of the same order while the vevs satisfy $v_2 \gg v_3$, we get the desired form of the pattern $C1$ [Eq. (73)] with $\chi = \frac{-2v_3 B^3}{v_2 B^2 + v_3 B^3}$.

3. Charged lepton mass matrix—flavor basis

We need here to extend the symmetry to the charged lepton sector and arrange the couplings in order to be in the "flavor basis" where the charged lepton mass matrix is diagonal. For this we present three possible options.

(1) Just the SM Higgs boson

We have the usual Yukawa coupling term,

$$\mathcal{L}_1 = Y_{ij}\bar{L}_i\Phi l^c_j. \tag{90}$$

We assume the SM Higgs Φ is singlet under the flavor symmetry,

$$\Phi \xrightarrow{S} \Phi, \qquad \Phi \xrightarrow{Z_2} \Phi, \tag{91}$$

and present two scenarios for the RH charged lepton singlets' l^c_j transformation under $S \times Z_2$ as follows:

(i) l^c_j transforms similarly as L

We assume

$$l^c \xrightarrow{S} S l^c, \qquad l^c \xrightarrow{Z_2} \mathrm{diag}(1,-1,-1) l^c. \tag{92}$$

We then get, via Eqs. (81), (91), and (92),

$$S^{\mathrm{T}} Y S = Y, \qquad \bar{L}_i l^c_j \overset{Z_2}{\sim} \begin{pmatrix} 1 & -1 & -1 \\ -1 & 1 & 1 \\ -1 & 1 & 1 \end{pmatrix}, \tag{93}$$

which would lead, upon acquiring a vev v for the SM Higgs boson, to a charged lepton mass matrix of the form [see Eqs. (77) and (93)]

$$M_l = v \begin{pmatrix} A & 0 & 0 \\ 0 & C & D \\ 0 & D & C \end{pmatrix} \Rightarrow M_l M_l^\dagger = v^2 \begin{pmatrix} |A|^2 & 0 & 0 \\ 0 & |C|^2 + |D|^2 & 2\Re(CD^*) \\ 0 & 2\Re(CD^*) & |C|^2 + |D|^2 \end{pmatrix}. \tag{94}$$

Thus, we need to perform a rotation across the 1^{st} axis by an angle $\theta_y = \pi/4$ in order to diagonalize the squared charged lepton mass matrix and be in the flavor basis. Thus, this option is not interesting since it spoils the neutrino mixing predictions carried out in the flavor basis.

(ii) l^c_j is singlet under flavor symmetry

We assume

$$l^c \xrightarrow{S} l^c, \qquad l^c \xrightarrow{Z_2} l^c. \tag{95}$$

We then get, via Eqs. (81), (91), and (95),

$$SY = Y, \qquad \bar{L}_i l^c_j \overset{Z_2}{\sim} \begin{pmatrix} 1 & 1 & 1 \\ -1 & -1 & -1 \\ -1 & -1 & -1 \end{pmatrix}, \tag{96}$$

which would lead, upon acquiring a vev v for the SM Higgs boson, to a charged lepton mass matrix of the form [see Eqs. (79) and (96)

$$M_l = v \begin{pmatrix} A & B & C \\ 0 & 0 & 0 \\ 0 & 0 & 0 \end{pmatrix} \Rightarrow M_l M_l^\dagger = v^2 \begin{pmatrix} |A|^2 + |B|^2 + |C|^2 & 0 & 0 \\ 0 & 0 & 0 \\ 0 & 0 & 0 \end{pmatrix}. \tag{97}$$

The squared mass matrix is diagonal, but it predicts two vanishing eigen masses for the 2nd and 3rd families, which is not acceptable experimentally.

(2) Three SM-like Higgs doublets

We extend the SM to include three scalar doublets ϕ_k playing the role of the ordinary SM-Higgs boson field. The Lagrangian responsible for the charged lepton mass is given by

$$\mathcal{L}_2 = f^j_{ik}\bar{L}_i\phi_k l^c_j. \tag{98}$$

We assume the Higgs fields ϕ_k, $k = 1, 2, 3$ transforms as L_i under $S \times Z_2$:

$$\phi \xrightarrow{S} S\phi, \qquad \phi \xrightarrow{Z_2} \mathrm{diag}(1,-1,-1)\phi. \tag{99}$$

Equally, the RH charged leptons are supposed to transform as singlets under S:

$$l^c \xrightarrow{S} l^c, \tag{100}$$

whereas we present two scenarios for their transformations under Z_2 as follows.

(i) l^c_j transforms similarly as L under Z_2

We assume

$$l^c \xrightarrow{Z_2} \mathrm{diag}(1,-1,-1) l^c. \tag{101}$$

We then get, via Eqs. (81), (99), (100), and (101),

$$S^{\mathrm{T}} f^{(j)} S = f^{(j)}, \qquad \bar{L}_i \phi_k \overset{Z_2}{\sim} \begin{pmatrix} 1 & -1 & -1 \\ -1 & 1 & 1 \\ -1 & 1 & 1 \end{pmatrix}, \tag{102}$$

where $f^{(j)}$ is the matrix whose $(i,k)^{th}$ entry is the Yukawa coupling f^j_{ik}. Then Eqs. (77), (101), and

(102) lead to the following forms of the Yukawa coupling matrices:

$$f^{(1)}=\begin{pmatrix} A^1 & 0 & 0\\ 0 & C^1 & D^1\\ 0 & D^1 & C^1\end{pmatrix},\quad f^{(2)}=\begin{pmatrix} 0 & B^2 & B^2\\ E^2 & 0 & 0\\ E^2 & 0 & 0\end{pmatrix},$$
$$f^{(3)}=\begin{pmatrix} 0 & B^3 & B^3\\ E^3 & 0 & 0\\ E^3 & 0 & 0\end{pmatrix}. \tag{103}$$

If there is acute hierarchy in the vevs, $v_3 \gg v_1, v_2$, say, we get, for real entries, a charged lepton mass matrix of the form

$$M_l = v_3\begin{pmatrix} 0 & B^2 & B^3\\ D^1 & 0 & 0\\ C^1 & 0 & 0\end{pmatrix}. \tag{104}$$

We see that this choice of Z_2-charge assignments for the RH lepton singlets leads to one vanishing mass, which is excluded by experiment. Thus, we turn to the other choice which would prove capable of producing the charged lepton mass spectrum.

(ii) l^c_j transforms differently from L under Z_2
We assume

$$l^c \xrightarrow{Z_2} \mathrm{diag}(1,1,-1)l^c. \tag{105}$$

We get the same Eq. (102), but Eq. (105) now leads to

$$f^{(1)}=\begin{pmatrix} A^1 & 0 & 0\\ 0 & C^1 & D^1\\ 0 & D^1 & C^1\end{pmatrix},\quad f^{(2)}=\begin{pmatrix} A^2 & 0 & 0\\ 0 & C^2 & D^2\\ 0 & D^2 & C^2\end{pmatrix},$$
$$f^{(3)}=\begin{pmatrix} 0 & B^3 & B^3\\ E^3 & 0 & 0\\ E^3 & 0 & 0\end{pmatrix}. \tag{106}$$

The hierarchy ($v_3 \gg v_1, v_2$) would now lead to the following form for the charged lepton mass matrix:

$$M_l = v_3\begin{pmatrix} 0 & 0 & B^3\\ D^1 & D^2 & 0\\ C^1 & C^2 & 0\end{pmatrix} \Rightarrow M_l M_l^\dagger$$
$$= v_3^2\begin{pmatrix} |\mathbf{B}|^2 & 0 & 0\\ 0 & & |\mathbf{D}|^2 \quad \mathbf{D}\cdot\mathbf{C}\\ 0 & \mathbf{C}\cdot\mathbf{D} & |\mathbf{C}|^2\end{pmatrix}, \tag{107}$$

where $\mathbf{B}=(0,0,B^3)^T$, $\mathbf{D}=(D^1,D^2,0)^T$, and $\mathbf{C}=(C^1,C^2,0)^T$, and where the dot product is defined as $\mathbf{D}\cdot\mathbf{C}=\sum_{i=1}^{i=3} D^i C^{i*}$. Now one can adjust the Yukawa couplings to require an infinitesimal rotation in order to diagonalize the squared charged lepton mass matrix and be in the flavor basis. In fact, let us just assume the magnitudes of the three vectors coming in ratios comparable to the lepton mass ratios:

$$\frac{|\mathbf{B}|}{|\mathbf{C}|}\equiv\lambda_e\sim\frac{m_e}{m_\tau}=2.8\times10^{-4},$$
$$\frac{|\mathbf{D}|}{|\mathbf{C}|}\equiv\lambda_\mu\sim\frac{m_\mu}{m_\tau}=5.9\times10^{-2}. \tag{108}$$

Then it is easy to see that the matrix

$$U(\theta,\alpha,\beta)=\begin{pmatrix} 1 & 0 & 0\\ 0 & c_\theta e^{-i\alpha} & s_\theta e^{-i\beta}\\ 0 & -s_\theta e^{-i\alpha} & c_\theta e^{-i\beta}\end{pmatrix}: \tag{109}$$

$$\alpha-\beta=\arg(\mathbf{D}\cdot\mathbf{C}),$$
$$\tan 2\theta=\frac{2\mathbf{D}\cdot\mathbf{C}}{|\mathbf{D}|^2-|\mathbf{C}|^2}\simeq 2\frac{|\mathbf{D}|}{|\mathbf{C}|}\cos\psi, \tag{110}$$

where ψ is the angle between the two complex vectors $\mathbf{D}$ and $\mathbf{C}$, defined by $\cos\psi=\mathbf{D}\cdot\mathbf{C}/(|\mathbf{D}|\cdot|\mathbf{C}|)$, does diagonalize $M_l M_l^\dagger$. Note that one can absorb the individual phases α, β using the freedom of multiplying the unitary diagonalizing matrix by a diagonal phase matrix, which would leave us with only one "physical" phase $\alpha-\beta$:

$$U(\theta,\alpha,\beta)=\begin{pmatrix} 1 & 0 & 0\\ 0 & c_\theta & s_\theta e^{-i(\beta-\alpha)}\\ 0 & -s_\theta e^{i(\beta-\alpha)} & c_\theta\end{pmatrix}. \tag{111}$$

Thus, we are in the flavor basis, as required, up to an infinitesimal rotation of an angle less than 10^{-2} [see Eqs. (108) and (110)].

(3) SM plus three Higgs boson singlets
One might keep the SM Higgs doublet Φ, with the same flavor transformations of Eq. (91), but add three Higgs singlets Δ_k in order to contribute to the charged lepton mass through dimension-five operators. The Lagrangian responsible for the charged lepton mass is given by

$$\mathcal{L}_4=\mathcal{L}_1+\mathcal{L}_3=Y_{ij}\bar{L}_i\Phi l^c_j+\frac{g^j_{ik}}{\Lambda}\bar{L}_i\Phi\Delta_k l^c_j, \tag{112}$$

where Λ is a mass high scale characterizing the Higgs singlets. We assume the Higgs singlet fields Δ_k, $k=1$, 2, 3 transform as L_i under $S\times Z_2$:

$$\Delta \xrightarrow{S} S\Delta, \qquad \Delta \xrightarrow{Z_2} \mathrm{diag}(1,-1,-1)\Delta. \tag{113}$$

As in the previous enumeration, the RH charged leptons are supposed to be singlets under S [Eq. (100)], whereas for Z_2 we have the following options:

(i) l_j^c transforms similarly as L under Z_2
We thus have Eq. (101). The invariance of $\mathcal{L}_1$ implies

$$SY = Y, \qquad \bar{L}_i l_j^c \overset{Z_2}{\sim} \begin{pmatrix} 1 & -1 & -1 \\ -1 & 1 & 1 \\ -1 & 1 & 1 \end{pmatrix}. \tag{114}$$

This leads, when Φ acquires a vev, to a contribution to the mass matrix [see Eqs. (79) and (93)]:

$$M_1 = \begin{pmatrix} a & 0 & 0 \\ 0 & e & f \\ 0 & e & f \end{pmatrix}. \tag{115}$$

Equation (113) would lead, exactly as the three Higgs doublets did in the previous enumeration, to a mass contribution M_2 of the form of Eq. (104) when the Higgs singlets acquire vevs (δ_k), with the hierarchy $\delta_3 \gg \delta_1, \delta_2$. Thus, we get the charged lepton mass matrix in the form

$$M_l = M_1 + M_2 = \begin{pmatrix} a & B^2 & B^3 \\ D^1 & e & f \\ C^1 & e & f \end{pmatrix}, \tag{116}$$

with the condition that $D^1 \neq C^1$ in order not to make the determinant of the matrix equal to zero, implying a vanishing mass.

(ii) l_j^c transforms differently from L under Z_2
We thus have Eq. (105). The invariance of $\mathcal{L}_1$ implies

$$SY = Y, \qquad \bar{L}_i l_j^c \overset{Z_2}{\sim} \begin{pmatrix} 1 & 1 & -1 \\ -1 & -1 & 1 \\ -1 & -1 & 1 \end{pmatrix}, \tag{117}$$

so when Φ acquires a vev we get a contribution to the mass matrix [see Eqs. (79) and (117)]:

$$M_1 = \begin{pmatrix} a & b & 0 \\ 0 & 0 & f \\ 0 & 0 & f \end{pmatrix}. \tag{118}$$

Equation (113) would lead, exactly as the three Higgs doublets did in the previous case, to a mass contribution M_2 of the form of Eq. (107) when the Higgs singlets acquire vevs (δ_k), with the hierarchy $\delta_3 \gg \delta_1, \delta_2$. Thus, we get the charged lepton mass matrix in the form

$$M_l = M_1 + M_2 = \begin{pmatrix} a & b & B^3 \\ D^1 & D^2 & f \\ C^1 & C^2 & f \end{pmatrix}. \tag{119}$$

(iii) In both previous items we get a charged lepton mass matrix of the form

$$M_l = \begin{pmatrix} \mathbf{A}^T \\ \mathbf{B}^T \\ \mathbf{C}^T \end{pmatrix}, \tag{120}$$

which is adjustable so that the three vectors are linearly independent, making the mass matrix invertible. The discussion in [41] on the charged lepton mass matrix of the same form showed the possibility of adjusting Yukawa couplings in order to get the charged lepton mass hierarchy, and then, automatically, the working basis will become the flavor basis up to the order λ_μ. We shall not repeat the same analysis here, but just note that in the case that the parameters a, b, f (corresponding to $\mathcal{L}_1$) are negligible compared to B, C, D (related to $\mathcal{L}_3$), the last item [Eq. (119)] is similar to the last item of the past enumeration [Eq. (107)], where we explicitly showed the charged lepton mass diagonalizing matrix being an infinitesimal rotation, which allows us to consider the matrices as being those in the flavor basis, with a good approximation.

Before we finish this subsection, we note that there is an advantage for using the type II seesaw mechanism in that the flavor changing neutral current due to the triplet is highly suppressed because of the heaviness of the triplet mass scale, or, equivalently, the smallness of the neutrino masses.

B. Type I seesaw

We proceed now to find a realization of the perturbed texture of the pattern C1 [Eq. (73)] in the type I seesaw mechanism where the effective neutrino mass matrix (M_ν) is expressed in terms of the Dirac neutrino mass matrix (M_D) and the RH Majorana neutrino mass matrix (M_R) through

$$M_\nu = M_D M_R^{-1} M_D^T. \tag{121}$$

For the flavor symmetry, we start by adding a new Z_2 symmetry (called Z_2') to the flavor symmetry of the type II case, but we shall see that it is not enough to

achieve the desired form, and needs to be expanded to a larger group (say to $S \times Z_8$) for this.

1. $S \times Z_2 \times Z_2'$-flavor symmetry

We consider here a minimal extension to the flavor group of the type II seesaw by adding a new Z_2 symmetry in order to get the group $(Z_2)^3$.

(1) Matter content and symmetry transformations
We have three SM-like Higgs doublets (ϕ_i, $i = 1, 2, 3$) that would give mass to the charged leptons and another three Higgs doublets (ϕ_i', $i = 1, 2, 3$) for the Dirac neutrino mass matrix. The RH neutrinos are denoted by (ν_{Ri}, $i = 1, 2, 3$). These fields transform as follows:

$$\nu_R \xrightarrow{Z_2'} -\nu_R, \qquad \phi' \xrightarrow{Z_2'} -\phi' \tag{122}$$

$$L \xrightarrow{Z_2'} L, \qquad l^c \xrightarrow{Z_2'} l^c, \qquad \phi \xrightarrow{Z_2'} \phi, \tag{123}$$

$$\nu_R \xrightarrow{Z_2} \mathrm{diag}(1,-1,-1)\nu_R, \qquad \phi' \xrightarrow{Z_2} \mathrm{diag}(1,-1,-1)\phi' \tag{124}$$

$$L \xrightarrow{Z_2} \mathrm{diag}(1,-1,-1)L, \qquad l^c \xrightarrow{Z_2} \mathrm{diag}(1,1,-1)l^c,$$
$$\phi \xrightarrow{Z_2} \mathrm{diag}(1,-1,-1)\phi, \tag{125}$$

$$\nu_R \xrightarrow{S} S\nu_R, \qquad \phi' \xrightarrow{S} \mathrm{diag}(1,1,-1)\phi' \tag{126}$$

$$L \xrightarrow{S} SL, \qquad l^c \xrightarrow{S} l^c, \qquad \phi \xrightarrow{S} S\phi. \tag{127}$$

(2) Charged lepton mass matrix-flavor basis
As was the case of type-II seesaw with three SM-like Higgs doublets and where the RH charged lepton singlets transform differently from L under Z_2, the Lagrangian responsible for the charged lepton mass is given by Eq. (98). The Z_2' does not play a role here, since all the fields involved are singlets under it, except for the fact that it does forbid the trilinear coupling between ϕ', L, and l^c. Again, assuming a hierarchy in the Higgs ϕ's fields vevs ($v_3 \gg v_2, v_1$), we end up with a charged lepton mass matrix of the form [Eq. (107)] that can be adjusted to be in the flavor basis to a good approximation.

(3) The Dirac neutrino mass matrix
The Lagrangian responsible for the neutrino mass matrix is

$$\mathcal{L}_D = g_{ij}^k \bar{L}_i \tilde{\phi}'_k \nu_{Rj}, \quad \text{where } \tilde{\phi}' = i\sigma_2 \phi'^*. \tag{128}$$

This Lagrangian is clearly invariant under Z_2' [see Eq. (122)], which forces the existence of ϕ' rather than ϕ in $\mathcal{L}_D$. For the $S \times Z_2$ factor, we then get, via Eqs. (124), (125), (126), and (127),

$$S^{\mathrm{T}} g^{(k=1,2)} S = g^{(k=1,2)},$$
$$S^{\mathrm{T}} g^{(k=3)} S = -g^{(k=3)},$$
$$\bar{L}_i \nu_{Rj} \overset{Z_2}{\sim} \begin{pmatrix} 1 & -1 & -1 \\ -1 & 1 & 1 \\ -1 & 1 & 1 \end{pmatrix}, \tag{129}$$

where $g^{(k)}$ is the matrix whose $(i,j)^{th}$ entry is the Yukawa coupling g_{ij}^k. Then Eqs. (77), (78), (124), and (129) lead to the following forms of the Yukawa coupling matrices:

$$g^{(1)} = \begin{pmatrix} A^1 & 0 & 0 \\ 0 & C^1 & D^1 \\ 0 & D^1 & C^1 \end{pmatrix}, \quad g^{(2)} = \begin{pmatrix} 0 & B^2 & B^2 \\ E^2 & 0 & 0 \\ E^2 & 0 & 0 \end{pmatrix},$$
$$g^{(3)} = \begin{pmatrix} 0 & B^3 & -B^3 \\ E^3 & 0 & 0 \\ -E^3 & 0 & 0 \end{pmatrix}. \tag{130}$$

Upon acquiring vevs (v_i', $i = 1, 2, 3$) for the Higgs fields (ϕ_i'), we get the following Dirac neutrino mass matrix:

$$M_D = \Sigma_{k=1}^{k=3} v_k' g^{(k)} = \begin{pmatrix} A_D & B_D & B_D(1+\alpha) \\ E_D & C_D & D_D \\ E_D(1+\beta) & D_D & C_D \end{pmatrix}, \tag{131}$$

with

$$\alpha = \frac{-2v_3' B^3}{v_2' B^2 + v_3' B^3}, \qquad \beta = \frac{-2v_3' E^3}{v_2' E^2 + v_2' E^3}. \tag{132}$$

If the vevs satisfy $v_3' \ll v_2'$ and the Yukawa couplings are of the same order, then we get the perturbative parameters $\alpha, \beta \ll 1$.

(4) Majorana neutrino mass matrix
The mass term is directly present in the Lagrangian

$$\mathcal{L}_R = M_{Rij} \nu_{Ri} \nu_{Rj}. \tag{133}$$

It is invariant under Z_2'. Then Eqs. (126) and (124) lead to

$$S^{T}M_{R}S=M_{R},$$
$$\nu_{Ri}\nu_{Rj}\overset{Z_2}{\sim}\begin{pmatrix}1&-1&-1\\-1&1&1\\-1&1&1\end{pmatrix}\overset{\text{Eq.75}}{\Rightarrow}M_{R}=\begin{pmatrix}A_R&0&0\\0&C_R&D_R\\0&D_R&C_R\end{pmatrix}. \quad (134)$$

(5) Effective neutrino mass matrix
One can see by direct computation that plugging Eqs. (131) and (134) in the seesaw formula [Eq. (121)] would result in an effective neutrino mass matrix of the form

$$M_{\nu}=\begin{pmatrix}M_{\nu 11}&M_{\nu 12}&M_{\nu 12}(1+\chi)\\M_{\nu 12}&M_{\nu 22}&M_{\nu 23}\\M_{\nu 12}(1+\chi)&M_{\nu 23}&M_{\nu 22}(1+\xi)\end{pmatrix}, \quad (135)$$

where $(Y=A,B,C,D,E)$

$$\chi=\chi(\alpha,\beta,Y_D,Y_R),$$
$$\xi=\xi(\beta,Y_D,Y_R):\ \beta=0\Rightarrow\xi=0. \quad (136)$$

Thus, in general, we do not get the desired $C1$-pattern form [Eq. (73)] corresponding to $\xi=0$. However, for some choices of the Yukawa couplings satisfying $E^3=0$ we get this form [see Eq. (132)], with χ, as α is a small parameter for moderate values of Yukawa couplings.

2. $S\times Z_8$-flavor symmetry

In order to get a realization of the $C1$ pattern form with no need to tune the Yukawa couplings, we extend the flavor symmetry to be $S\times Z_8$.

(1) Matter content and symmetry transformations
The matter spectrum consists of three SM-like Higgs doublets (ϕ_i, $i=1,2,3$) responsible for the charged lepton masses, and of four Higgs doublets (ϕ'_j, $j=1,2,3,4$) giving rise when acquiring a vev to the Dirac neutrino mass matrix, and, as before, of left doublets (L_i, $i=1,2,3$), RH charged singlets (l^c_j, $j=1,2,3$), and RH neutrinos (ν_{Rj}, $j=1,2,3$). We also introduce two Higgs singlet scalars (Δ_k, $k=1,2$) related to the Majorana neutrino mass matrix. We denote the octic root of the unity by $w=e^{\frac{i\pi}{4}}$. The fields transform under the flavor symmetry as follows:

$$L\overset{S}{\longrightarrow}SL,\qquad l^c\overset{S}{\longrightarrow}l^c,\qquad \phi\overset{S}{\longrightarrow}S\phi, \quad (137)$$

$$\nu_R\overset{S}{\longrightarrow}S\nu_R,\qquad \phi'\overset{S}{\longrightarrow}\mathrm{diag}(1,1,1,-1)\phi',\qquad \Delta\overset{S}{\longrightarrow}\Delta \quad (138)$$

$$L\overset{Z_8}{\longrightarrow}\mathrm{diag}(1,-1,-1)L,\qquad l^c\overset{Z_8}{\longrightarrow}\mathrm{diag}(1,1,-1)l^c,$$
$$\phi\overset{Z_8}{\longrightarrow}\mathrm{diag}(1,-1,-1)\phi, \quad (139)$$

$$\nu_R\overset{Z_8}{\longrightarrow}\mathrm{diag}(w,w^3,w^3)\nu_R,\quad \phi'\overset{Z_8}{\longrightarrow}\mathrm{diag}(w,w^3,w^7,w^3)\phi',$$
$$\Delta\overset{Z_8}{\longrightarrow}\mathrm{diag}(w^6,w^2)\Delta. \quad (140)$$

Note here that we have the following transformation rule for $\tilde{\phi}'\equiv i\sigma_2\phi'^{*}$:

$$\tilde{\phi}'\overset{S}{\longrightarrow}\mathrm{diag}(1,1,1,-1)\tilde{\phi}',$$
$$\tilde{\phi}'\overset{Z_8}{\longrightarrow}\mathrm{diag}(w^7,w^5,w,w^5)\tilde{\phi}'. \quad (141)$$

(2) Charged lepton mass matrix-flavor basis
As in the previous case of $S\times Z_2\times Z'_2$-flavor symmetry, the charged lepton mass Lagrangian is given again by Eq. (98). Since the transformations of the involved fields (L,l^c,ϕ) are identical under S in both flavor symmetry groups and are equally the same under Z_8 (in $S\times Z_8$) compared to Z_2 (in $S\times Z_2\times Z'_2$), we end up, assuming again a hierarchy in the Higgs ϕ's fields vevs ($v_3\gg v_2,\ v_1$), with a charged lepton mass matrix of the form [Eq. (107)] adjustable to be approximately in the flavor basis. Also note here that no terms of the form $f^{kl}_{ij}\bar{L}_i\phi'_k l^c_j$ can exist since we have

$$\bar{L}_i l^c_j\overset{Z_8}{\sim}\begin{pmatrix}1&1&-1\\-1&-1&1\\-1&-1&1\end{pmatrix}\overset{\text{Eq.140}}{\Rightarrow}\nexists i,j,k:$$
$$\bar{L}_i\phi'_k l^c_j=Z_8(\bar{L}_i\phi'_k l^c_j). \quad (142)$$

(3) The Dirac neutrino mass matrix
The Lagrangian responsible for the neutrino mass matrix is again given by Eq. (128). By means of Eqs. (137), (138), (139), (140), and (141), we have

$$S^{T}g^{(k=1,2)}S=g^{(k=1,2,3)},$$
$$S^{T}g^{(k=4)}S=-g^{(k=4)},$$
$$\bar{L}_i\nu_{Rj}\overset{Z_8}{\sim}\begin{pmatrix}w&w^3&w^3\\w^5&w^7&w^7\\w^5&w^7&w^7\end{pmatrix}, \quad (143)$$

where, as before, $g^{(k)}$ is the matrix whose $(i,j)^{th}$ entry is the Yukawa coupling g^k_{ij}. Then Eqs. (77), (78), (141), and (143) impose the following forms on the Yukawa coupling matrices:

$$g^{(1)}=\begin{pmatrix} A^1 & 0 & 0\\ 0 & 0 & 0\\ 0 & 0 & 0\end{pmatrix},\quad g^{(2)}=\begin{pmatrix} 0 & B^2 & B^2\\ 0 & 0 & 0\\ 0 & 0 & 0\end{pmatrix},$$
$$g^{(3)}=\begin{pmatrix} 0 & 0 & 0\\ 0 & C^3 & D^3\\ 0 & D^3 & C^3\end{pmatrix},\quad g^{(4)}=\begin{pmatrix} 0 & B^4 & -B^4\\ 0 & 0 & 0\\ 0 & 0 & 0\end{pmatrix}. \tag{144}$$

When the Higgs fields (ϕ'_i) get vevs $(v'_i, i=1,2,3,4)$, we obtain the following Dirac neutrino mass matrix:

$$M_D=\Sigma_{k=1}^{k=4}v'_k g^{(k)}=\begin{pmatrix} A_D & B_D & B_D(1+\alpha)\\ 0 & C_D & D_D\\ 0 & D_D & C_D\end{pmatrix}, \tag{145}$$

with

$$\alpha=\frac{-2v'_4B^4}{v'_2B^2+v'_4B^4}. \tag{146}$$

If the vevs satisfy $v'_4 \ll v'_2$ and the Yukawa couplings are of the same order, then we get a perturbative parameter $\alpha \ll 1$.

(4) Majorana neutrino mass matrix
The mass term is generated from the Lagrangian

$$\mathcal{L}_R=h^k_{ij}\Delta_k\nu_{Ri}\nu_{Rj}. \tag{147}$$

Under Z_8 we have the bilinear

$$\nu_{Ri}\nu_{Rj}\overset{Z_8}{\sim}\begin{pmatrix} w^2 & w^4 & w^4\\ w^4 & w^6 & w^6\\ w^4 & w^6 & w^6\end{pmatrix}\overset{\text{Eq.(140)}}{\Rightarrow}$$
$$\mathcal{L}_R=h^1_{11}\Delta_1\nu_{R1}\nu_{R1}+h^2_{11}\Delta_2\nu_{R2}\nu_{R2}+h^2_{23}\Delta_2\nu_{R2}\nu_{R3}+h^2_{32}\Delta_2\nu_{R3}\nu_{R2}+h^2_{33}\Delta_2\nu_{R3}\nu_{R3}. \tag{148}$$

If we call $h^{(k)}$ the matrix whose $(i,j)^{th}$ entry is the coupling h^k_{ij}, then we have (with the cross sign denoting a nonvanishing entry)

$$h^{(1)}=\begin{pmatrix} \times & 0 & 0\\ 0 & 0 & 0\\ 0 & 0 & 0\end{pmatrix},\qquad h^{(2)}=\begin{pmatrix} 0 & 0 & 0\\ 0 & \times & \times\\ 0 & \times & \times\end{pmatrix}. \tag{149}$$

Then Eq. (138) leads to

$$S^{\mathrm{T}}h^{(k)}S=h^{(k)},\overset{\text{Eqs.75,149}}{\Rightarrow}h^{(1)}=\begin{pmatrix} a_R & 0 & 0\\ 0 & 0 & 0\\ 0 & 0 & 0\end{pmatrix},$$
$$h^{(2)}=\begin{pmatrix} 0 & 0 & 0\\ 0 & c_R & d_R\\ 0 & d_R & c_R\end{pmatrix}. \tag{150}$$

Thus, when the Higgs singlets Δ acquire vevs (δ^0_1,δ^0_2) we get the Majorana neutrino mass matrix

$$M_R=\sum_{k=1}^{2}\delta^0_k h^{(k)}=\begin{pmatrix} A_R & 0 & 0\\ 0 & C_R & D_R\\ 0 & D_R & C_R\end{pmatrix}. \tag{151}$$

(5) Effective neutrino mass matrix
By direct computation, plugging Eqs. (145) and (151) into the seesaw formula [Eq. (121)] results in an effective neutrino mass matrix of the desired $C1$-pattern form

$$M_\nu=\begin{pmatrix} M_{\nu 11} & M_{\nu 12} & M_{\nu 12}(1+\chi)\\ M_{\nu 12} & M_{\nu 22} & M_{\nu 23}\\ M_{\nu 12}(1+\chi) & M_{\nu 23} & M_{\nu 22}\end{pmatrix}, \tag{152}$$

where the perturbation parameter χ is given by

$$\chi=\frac{\alpha(C_D-D_D)(C_R+D_R)}{(1+\alpha)(C_RD_D-D_RC_D)+C_RC_D-D_RD_D}. \tag{153}$$

Before ending this section, we would mention that introducing multiple Higgs doublets as we did in our constructions might display flavor-changing neutral currents. However, the effects are calculable in the models and, in principle, one can adjust the Yukawa couplings so that processes like $\mu\to e\gamma$ are suppressed [42]. Moreover, and as was discussed in the introduction, the RG running effects are expected to be small when multiple Higgs doublets are present, so as not to spoil the predictions of the symmetry at low scale.

X. SUMMARY AND DISCUSSION

We have carried out a thorough phenomenological analysis for the patterns of the neutrino mass matrix meeting the μ–τ symmetry. We found that exact symmetry

leads to a totally degenerate spectrum and so is excluded on phenomenological grounds.

We thus introduced, in a minimal way, perturbations such that the neutrino mass matrix satisfies an approximate μ–τ symmetry. We got four such patterns and carried out a complete phenomenological analysis of them. We found that all these "deformed" patterns can accommodate the current data without the need to adjust the input parameters. However, no singular such patterns could meet the experimental constraints.

All the four patterns can produce all types of hierarchy and all have complex entries able to show *CP*-violation effects. The mixing angle θ_x can cover all of its admissible range in all four patterns. As to the angle θ_y, it is unconstrained in the patterns C3 except that it should not equal the value 45°, whereas it is restricted to be around 45°, without taking this value, in the C1 pattern for the normal and inverted hierarchies, and around 36° or 52° in the C4 pattern of the normal hierarchy type. Again, θ_y cannot take the value 45° in the C2 pattern of the normal or inverted hierarchy types, where it is just mildly constrained in the normal type to be around 45°. However, for this latter pattern C2, the mixing angle θ_z cannot be larger than 10°. Actually, there is a narrow interval $]4°, 4.7°[$ for θ_z in the C4 pattern of the normal type, whereas this mixing angle is bounded by 8° in the inverted type.

The phases are not constrained in the C3 or C4 patterns, except that in the C4 pattern of the normal type the Dirac phase δ cannot be in the interval $]160°, 185°[$ and the Majorana phase $\rho(\mathrm{mod}\,\pi)$ cannot belong to $]-20°, 20°[$. As to the C1 pattern of the normal type, the phases σ, $\rho(\mathrm{mod}\,\pi)$ cannot take values in the interval $]-4°, 4°[$ around the origin, whereas the Dirac phase δ in all hierarchy types is excluded from a narrow band $]177°, 180.5°[$ around π. For the C2 pattern, the phase ρ is excluded from the interval $]94°, 99°[$ in the degenerate case, and from broader intervals in the normal $(]90°, 111°[)$ and inverted $(]48°, 137°[)$ types. The phase $\sigma(\mathrm{mod}\,\pi)$ is bound not to be around zero in the normal and inverted types, whereas the Dirac phase δ in all hierarchy types is excluded from narrow bands around zero $(]-3°, 1°[)$ and around π $(]178°, 185°[)$.

There exist linear correlations between δ, ρ, σ for the patterns C1 and C3 in all types of hierarchy, and a linear correlation between $\langle m_{ee}\rangle$ and the LNM in the degenerate type for these two patterns.

The strength of the hierarchies is characterized by the ratio m_{23}, and the normal type hierarchy is usually mild, taking values of the order 1 in all patterns. However, the inverted hierarchy type in the patterns C1 and C3 can be very acute, taking values of the order $O(10^2)$.

All these features might help in distinguishing between the independent patterns. For example, if by measuring the mass ratios we find a very pronounced hierarchy, then we know that we have either a C1 or C3 pattern of an inverted hierarchy type. Consequently, if by measuring the angle θ_y we find a value far from 45°, then we know we have a C3 pattern. Also, if δ gives a value around π then again we have a C3 pattern. On the other hand, if by measuring the masses we get a mild hierarchy, then we do not actually have enough signatures to determine the pattern. Rather, we have exclusion rules which help to drop as much patterns as possible. For example, if $\rho(\mathrm{mod}\,\pi) \in]-20°, 20°[$ or $\theta_z > 5°$ or $\theta_y \neq 36°, 52°$, then we can drop the C4 pattern of the normal type, whereas if $\theta_z > 8°$ we exclude the C4 of the inverted type possibility. If $|\rho(\mathrm{mod}\,\pi)| < 4°$, then there is no C1 pattern of the normal type, while if $\rho \in]94°, 99°[$, then we drop the possibility of a C2 pattern. Also, if $\theta_z \geq 10°$, then we conclude that we do not have a C2 pattern of the normal type. Moreover, the knowledge of all the phase angles and other mass parameters jointly and referring to the narrow bands of the correlation plots can help in deciding which texture does fit the data.

We note finally that the deformation parameter $|\chi|$ can cover all its perturbative range ($\lesssim 20\%$), except for the pattern C4 where it is bound to be a "tangible" deformation ($|\chi| \geq 16\%$) in order to fit the experimental data.

All the perturbed patterns can be realized assuming exact μ–τ symmetry augmented by new matter fields and Abelian symmetries at the Lagrangian level, and we have presented some concrete examples using both types I and II of the seesaw mechanism.

Our analysis follows a bottom-up approach and, in view of the full parameter space we adopted for the observables, can be considered as new. In particular, it shows in a very transparent way the correlation between the perturbation χ and the nonvanishing θ_z. We can summarize the mainly new results in our work as follows. First, we presented the complete analytical expressions (full or expanded) for all the observables and in all patterns. Second, we raised the question of convergence of the expansion series [Eq. (53)] and analyzed it. Third, we presented an exhaustive analysis plotting all the possible correlations. Fourth, we disentangled the effects of the two perturbation parameters and presented detailed theoretical realizations of the resulting perturbed patterns. Fifth, we also treated the case of the singular neutrino mass matrix. Sixth, we reached different conclusions compared to some other works with a far more restricted parameter space.

ACKNOWLEDGMENTS

Part of this work was done within the associate scheme and short visits program of ICTP. N. C. acknowledges funding provided by the Alexander von Humboldt Foundation.

[1] Y. Fukuda *et al.*, Phys. Lett. B **436**, 33 (1998); Phys. Rev. Lett. **81**, 1562 (1998); For a review, see Annu. Rev. Nucl. Part. Sci. **51**, 451 (2001).

[2] Q. R. Ahmad *et al.* (SNO Collaboration), Phys. Rev. Lett. **89**, 011301 (2002); **89**011302 (2002).

[3] K. Eguchi *et al.* (KamLAND Collaboration), Phys. Rev. Lett. **90**, 021802 (2003).

[4] M. H. Ahn *et al.* (K2K Collaboration), Phys. Rev. Lett. **90**, 041801 (2003).

[5] M. Apollonio *et al.* (CHOOZ Collaboration), Phys. Lett. B **420**, 397 (1998); F. Boehm *et al.* (Palo Verde Collaboration), Phys. Rev. Lett. **84**, 3764 (2000).

[6] K. Abe *et al.* (T2K Collaboration), Phys. Rev. Lett. **107**, 041801 (2011).

[7] P. Adamson *et al.* (MINOS Collaboration), Phys. Rev. Lett. **107**, 181802 (2011).

[8] Y. Abe *et al.* (DOUBLE-CHOOZ Collaboration), Phys. Rev. Lett. **108**, 131801 (2012).

[9] F. P. An *et al.* (DAYA-BAY Collaboration), Phys. Rev. Lett. **108**, 171803 (2012).

[10] J. K. Ahn *et al.* (RENO Collaboration), Phys. Rev. Lett. **108**, 191802 (2012).

[11] See, e.g., M. Hirsch, D. Meloni, S. Morisi, S. Pastor, E. Peinado, J. W. F. Valle, A. Adulpravitchai, D. Aristizabal Sierra *et al.*, arXiv:1201.5525.

[12] R. N. Mohapatra and S. Nussinov, Phys. Rev. D **60**, 013002 (1999); C. S. Lam, Phys. Lett. B **507**, 214 (2001); P. F. Harrison and W. G. Scott, Phys. Lett. B **547**, 219 (2002); T. Kitabayashi and M. Yasue, Phys. Rev. D **67**, 015006 (2003).

[13] W. Grimus and L. Lavoura, J. High Energy Phys. 07 (2001) 045; Phys. Lett. B **572**, 189 (2003); Y. Koide, Phys. Rev. D **69**, 093001 (2004); R. N. Mohapatra, J. High Energy Phys. 10 (2004) 027.

[14] P. F. Harrison, D. H. Perkins, and W. G. Scott, Phys. Lett. B **530**, 167 (2002).

[15] V. D. Barger, S. Pakvasa, T. J. Weiler, and K. Whisnant, Phys. Lett. B **437**, 107 (1998); A. J. Baltz, A. S. Goldhaber, and M. Goldhaber, Phys. Rev. Lett. **81**, 5730 (1998).

[16] C. H. Albright, A. Dueck, and W. Rodejohann, Eur. Phys. J. C **70**, 1099 (2010).

[17] Y. Kajiyama, M. Raidal, and A. Strumia, Phys. Rev. D **76**, 117301 (2007); L. L. Everett and A. J. Stuart, Phys. Rev. D **79**, 085005 (2009).

[18] E. Ma and M. Raidal, Phys. Rev. Lett. **87**, 011802 (2001); W. Grimus and L. Lavoura, J. High Energy Phys. 07 (2001) 045; E. Ma, Phys. Rev. D **66**, 117301 (2002); R. N. Mohapatra and S. Nasri, Phys. Rev. D **71**, 033001 (2005); R. N. Mohapatra, S. Nasri, and H.-B. Yu, Phys. Lett. B **615**, 231 (2005); S. Nasri, Int. J. Mod. Phys. A **20**, 6258 (2005); T. Kitabayashi and M. Yasue, Phys. Lett. B **621**, 133 (2005); S. Choubey and W. Rodejohann, Eur. Phys. J. C **40**, 259 (2005); R. N. Mohapatra, S. Nasri, and H. B. Yu, Phys. Lett. B **636**, 114 (2006); R. N. Mohapatra, S. Nasri, and H. B. Yu, Phys. Lett. B **639**, 318 (2006); Z.-z. Xing, H. Zhang, and S. Zhou, Phys. Lett. B **641**, 189 (2006); T. Ota and W. Rodejohann, Phys. Lett. B **639**, 322 (2006); Y. H. Ahn, S. K. Kang, C. S. Kim, and J. Lee, Phys. Rev. D **73**, 093005 (2006); I. Aizawa and M. Yasue, Phys. Rev. D **73**, 015002 (2006); K. Fuki and M. Yasue, Phys. Rev. D **73**, 055014 (2006); K. Fuki, M. Yasue, R. Jora, S. Nasri, and J. Schechter, Int. J. Mod. Phys. A **21**, 5875 (2006); K. Fuki and M. Yasue, Nucl. Phys. **B783**, 31 (2007); B. Adhikary, A. Ghosal, and P. Roy, J. High Energy Phys. 10 (2009) 040; Z. z. Xing and Y. L. Zhou, Phys. Lett. B **693**, 584 (2010); R. Jora, J. Schechter, and M. Naeem Shahid, Phys. Rev. D **80**, 093007 (2009); R. Jora, J. Schechter, and M. Naeem Shahid, Phys. Rev. D **82**, 079902 (2010); S.-F. Ge, H.-J. He, and F.-R. Yin, J. Cosmol. Astropart. Phys. 05 (2010) 017; I. de Medeiros Varzielas, R. González Felipe, and H. Serodio, Phys. Rev. D **83**, 033007 (2011); H.-J. He and F.-R. Yin, Phys. Rev. D **84**, 033009 (2011); Y. H. Ahn, H. Y. Cheng, and S. Oh, Phys. Lett. B **715**, 203 (2012); H.-J. He and X.-J. Xu, Phys. Rev. D **86**, 111301 (2012); S. Gupta, A. S. Joshipura, and K. M. Patel, J. High Energy Phys. 09 (2013) 035; B. Adhikary, M. Chakraborty, and A. Ghosal, J. High Energy Phys. 10 (2013) 043; C. Hamzaoui, S. Nasri, and M. Toharia, arXiv:1311.2188.

[19] M. Abbas and A. Y. Smirnov, Phys. Rev. D **82**, 013008 (2010).

[20] E. I. Lashin, M. Abbas, N. Chamoun, and S. Nasri, Phys. Rev. D **86**, 033013 (2012).

[21] E. I. Lashin, N. Chamoun, and S. Nasri, Phys. Rev. D **86**, 113013 (2012).

[22] J. Liao, D. Marfatia, and K. Whisnant, Phys. Rev. D **87**, 013003 (2013).

[23] S. Gupta, A. S. Joshipura, and K. M. Patel, J. High Energy Phys. 09 (2013) 035.

[24] B. Adhikary, A. Ghosal, and P. Roy, Int. J. Mod. Phys. A **28**, 1350118 (2013).

[25] A. S. Joshipura, Eur. Phys. J. C **53**, 77 (2007).

[26] R. N. Mohapatra and W. Rodejohann, Phys. Rev. D **72**, 053001 (2005); N. Haba and W. Rodejohann, Phys. Rev. D **74**, 017701 (2006); S. Luo and Z.-Z. Xing, Phys. Lett. B **646**, 242 (2007); Y. Koide and H. Nishiura, Int. J. Mod. Phys. A **25**, 3661 (2010).

[27] W. Grimus and L. Lavoura, Eur. Phys. J. C **39**, 219 (2005).

[28] A. Dighe, S. Goswami, and P. Roy, Phys. Rev. D **76**, 096005 (2007); S. Luo and Z.-z. Xing, Phys. Rev. D **86**, 073003 (2012).

[29] W. Grimus and L. Lavoura, Fortschr. Phys. **61**, 535 (2013).

[30] Z. Z. Xing, Phys. Lett. B **530**, 159 (2002).

[31] G. L. Fogli, E. Lisi, A. Marrone, A. Palazzo, and A. M. Rotunno, Phys. Rev. D **84**, 053007 (2011).

[32] E. Lashin and N. Chamoun, Phys. Rev. D **85**, 113011 (2012).

[33] C. Jarlskog, Phys. Rev. Lett. **55**, 1039 (1985); Z. Phys. C **29**, 491 (1985); Phys. Rev. D **35**, 1685 (1987).

[34] G. L. Fogli, E. Lisi, A. Marrone, D. Montanino, A. Palazzo, and A. M. Rotunno, Phys. Rev. D **86**, 013012 (2012).

[35] T. Schwetz, M. Tortola, and J. W. F. Valle, New J. Phys. **13**, 063004 (2011); T. Schwetz, M. Tortola, and J. W. F. Valle, New J. Phys. **13**, 109401 (2011); D. V. Forero, M. Tortola, and J. W. F. Valle, Phys. Rev. D **86**, 073012 (2012).

[36] M. C. Gonzalez-Garcia, M. Maltoni, and J. Salvado, J. High Energy Phys. 04 (2010) 056; M. C. Gonzalez-Garcia,

M. Maltoni, J. Salvado, and T. Schwetz, J. High Energy Phys. 12 (2012) 123.
[37] G. L. Fogli, E. Lisi, A. Marrone, A. Melchiorri, A. Palazzo, A. Rotunno, P. Serra, J. Silk, and A. Slosar, Phys. Rev. D **78**, 033010 (2008).
[38] E. Andreotti *et al.*, Astropart. Phys. **34**, 822 (2011).
[39] Z. Z. Xing, Phys. Rev. D **78**, 011301 (2008).
[40] T. P. Cheng and L. F. Li, Phys. Rev. D **22**, 2860 (1980); R. N. Mohapatra and G. Senjanovic, Phys. Rev. D **23**, 165 (1981).
[41] E. I. Lashin, N. Chamoun, E. Malkawi, and S. Nasri, Phys. Rev. D **83**, 013002 (2011).
[42] C. Hagedorn, J. Kersten, and M. Lindner, Phys. Lett. B **597**, 63 (2004).